Durham E-Theses

Application of computational fluid dynamics to turbo machinery unsteady aerodynamics and aero acoustics

Dong, Ying

How to cite:

Use policy

APPLICATION OF COMPUTATIONAL FLUID DYNAMICS TO TURBOMACHINERY UNSTEADY AERODYNAMICS AND AEROACOUSTICS

YING DONG

MSc

2008

0 6 OCT 2008

ABSTRACT

The aim of this thesis is to obtain numerical data for fan tone noise propagation and reducing the load from blade-tower interaction. By using a CFD code, MB3D, which is supplied by Professor Li He, fan tone noise transmission and wind turbine blade-tower interaction are simulated and analysed.

CFD application on turbomachinery unsteady flow is introduced and the two issues, fan tone noise and wind turbine have been reviewed. The CFD code to simulate the two different problems is introduced and its computational methodology is described.

By using CFD method, the sound wave transmission in cut-on and cut-off situations are simulated and analysed. The results show that when the disturbance frequency is above the cut-off frequency, the pressure wave can propagate along the duct, when the disturbance frequency is below the cut-off frequency, the pressure wave will decay along the duct. The different decay rates depend on different cut off ratio. The mesh dependency of the computational simulations has been examined.

Wind turbine blade-tower interaction is also simulated by using MB3D code. Adaptively pitching blade is introduced in order to minimize this interaction. The results show that with pitching blade by half degree or so, the unsteady forces on the blade can be at least halved, which can correspondingly reduce the bending moment (hence increase the fatigue life span), and improve the average power output.

Keywords: CFD, fan tone noise, cut-off, cut-on, cut-off frequency, pitch control, blade-tower interaction.

ACKNOWLEDGEMENTS

CONTENTS

LIST OF FIGURES

LIST OF TABLES

NOMENCLATURE

A	finite volume surface, m^2
e	specific internal energy, J/kg
q	heat flux
P	pressure, Pa
T	temperature, K
$\vec{n}$	unit vector
t	time, s
V	finite volume, m^3
U	conservative flow variable vector
F, G, H	inviscid fluxes
S	inviscid source term
x	axial coordinate, m
θ	tangential angular coordinate, rad
r	radial coordinate, m
τ	viscous stress
μ	dynamic viscosity, $Pa \cdot S$
κ	molecular thermal conductivity, $W/(m \cdot K)$
γ	specific heat ratio
ρ	density, kg/m^3
R_i	net inviscid fluxes through cell surfaces; Residual for the intermediate mesh
R_f	Residual for the fine mesh
R_c	Residual for the coarse mesh
R_v	net viscous fluxes through cell surfaces
a_n	Amplitude coefficient
ϕ_n	Phase angle

n	Harmonic number
B	Number of rotor blades
Ω	Rotor shaft speed, radians/sec
m	Number of lobes or cycles of circumferential pressure
f	driving frequency which can make the pressure wave transmit circumferentially;
$f_{m\mu}$	Cut-off frequency of (m, μ) mode
b	Outer wall radius;
M_m	Circumferential Mach number for m-lobe pattern,
$K_{m\mu}^{(\sigma)}$	Characteristic number depended on m, μ and σ.

Subscripts

m	moving grid
θ	tangential direction
r	radial direction
x	axial direction
f	the fine mesh
i	the intermediate mesh
c	the coarse mesh

Abbreviation

CFD	Computational Fluid Dynamics
CAA	Computational Aero Acoustic
CFL	Courant-Friedrich-Levy
BPF	Blade Passing Frequency
LES	Large Eddy Simulation
DNS	Direct Numerical Simulation

CHAPTER 1. INTRODUCTION

1.1 Overview of CFD Application on Turbomachinery Unsteady Flow

Computational Fluid Dynamics (CFD) is a method to solve and analyze problems which involve fluid flows by using numerical methods and algorithms. In recent 30 years, more and more people have been using CFD as a research and design tool to simulate and solve different kinds of issues related to fluid flows. Mechanical and manufacturing engineers improve the design of the vehicles by using CFD to analyze the external and internal flows of the vehicles in order to improve their performance; civil engineers are using CFD to analyze the structure and rheology of rivers and lakes as well; building service engineers are using CFD to set up the thermal modelling in order to provide comfortable and safe human environments. CFD has been widely used in more and more fields to solve problems (Anderson, 1995; Dixon, 1978). In the future, it is expected that surgeons will conduct operations which may affect the flow of fluids within the human body (blood, urine, air, the fluid within the brain) only after their probable effects have been predicted by CFD methods.

In turbomachinery field, CFD has been widely used to simulate unsteady flow situations due to the rotor-stator interaction, blade vibration, and blade trailing edge vortex shedding and so on. More and more advanced numerical methods

have been developed to be applied in the unsteady flow simulation in turbomachinery. Nonlinear time-marching method has been used for unsteady flow calculation from its birth. In this method, the time domain has a real meaning in which the unsteady or time-dependent solution is marched. For a periodic unsteady flow, such as the unsteady flow induced by bladerow interaction or blade vibration, the solution should be stepped through many cycles of the transient process until a periodic solution is reached. Usually, the time-marching unsteady calculation is much more CPU time consuming, however, the significant development of this method for unsteady turbomachinery flow has been made in last two decades, especially the application in the three areas: bladerow interactions, flutter, and trailing edge vortex shedding (Ning, 1998; Hanson, 1994). Giles proposed a novel phase-shift periodic boundary treatment in a wake/rotor interaction calculation where the flow governing equations are firstly transformed from the physical time domain to a computational time domain (Giles, 1988). Li He developed a time-consistent two-grid method which can considerably speed up the convergence of unsteady calculations (He, 1993). With the development of the CFD calculation method, the CFD application on unsteady flow is facilitated. Time-linearized harmonic method is an alternative to the nonlinear time-marching methods used for the unsteady flow analysis. In this method, an unsteady flow is decomposed into a steady flow plus a linear, harmonically varying unsteady perturbation. The harmonic perturbation equation is a linear equation with coefficients based on the steady flow solution. Currently, the time-linearized methods are being actively developed in three aspects which are to develop the 2D time-linearized Euler methods into fully three-dimensional methods (Hall and Lorence, 1992), to extend the Euler methods to Navier-Stokes methods (Holmes and Lorence, 1997), and to include the interaction effects from other blade rows in a single bladerow calculation. Although this method has high computational efficiency, the nonlinear effects are completely neglected due to the linear assumption which can be potentially important in turbomachinery unsteady flows. Nonlinear Harmonic Methodology has been recently proposed by He (He, 2006). In this

2

approach, the Time-Averaged flow (instead of steady flow) is used to be the base of unsteady perturbations. Nonlinear effects are to be included in a coupling solution between the time-averaged flow and included in a coupling solution which is the key to this nonlinear harmonic approach.

Recently, Computational Aeroacoustics (CAA) method has been developed as a viable tool for analysis of engineering problems in which noise plays a significant role. The promise of CAA lies in its ability to simulate accurately the physical processes involved in the generation and propagation of sound and thus it offers insights that can complement the knowledge gained from analytical and experimental methods. However, the noise issue is still a challenge to CAA due to its complexity. The application of CAA on fan noise will be reviewed in Chapter 2.

In this thesis, a computer code (MB3D) using CFD method is applied to solve the unsteady flow equations to predict fan tone noise, and also to simulate the wind-turbine blade-tower interaction. These problems and related issues are described in the next sections, and the CFD method is described in Chapter 3.

1.2 Problem Statement of CFD Application on Fan Tone Noise Prediction

Fan noise includes the broadband noise and tone noise. Fan tone noise is the main part of fan noise (caused by the rotating nonuniform pressure field around rotor blades). The prediction on the tone noise can contribute a lot to reduce the fan noise. In this thesis, the sound wave propagation in intake duct is simulated by using CFD method to analyse the different pressure wave transmission situations.

Why do we use CFD method to predict the fan tone noise? Analytical and experimental methods have been both used to analyse the fan noise problem. However, they both have the limitations. For the analytical methods, the theoretical models used in the fan tone noise prediction rely on simplified descriptions of configurations and flow conditions that prevail inside the engine. For the experimental methods, parametric studies tend to be expensive and time consuming. Therefore, the CFD method was introduced to apply for the analysis of this problem.

The main challenge to the nonlinear time-marching CFD method is the small acoustic signals relative to numerical errors. Acoustic waves usually have small amplitudes, which are very small compared to those of the mean flow. To compute sound waves accurately a numerical scheme must have low numerical dispersion and dissipation, which means they must have low numerical noise. CFD uses the Taylor series truncation error analysis, leading to that a higher order scheme is more accurate (less dissipative) than a lower order scheme. The basic elements in order to simulate this problem accurately are: time marching scheme, a suitably designed computation grid and a suitable numerical treatment for use at the boundaries of the computational domain (Tam, 2004). In this thesis, MB3D code was applied to simulate the sound wave transmission cut-on and cut-off 2D situations based on CFD method. The detail of this methodology will be described in chapter 3.

Currently, there is already the theory to predict the cut-on and cut-off situation in a simple 2D duct. However, for 3D situations, it is complicated. In 3D, there may well be that cut-on occurs for only a certain radial part and other regions along the radius are of a cut-off condition, when the sound waves transmit upstream in a duct. In order to simulate this, it is firstly necessary to simulate the 2D situation in order to identify if the methodology is applicable for this problem. And then, based on this, the MB3D code can be developed to be used to simulate the 3D

situation and predict the fan tone noise. Chapter 4 will discuss the cut-on and cut- off simulations.

1.3 Control of Wind Turbine Blade-Tower Interaction

Wind turbine is becoming more frequently used by different countries to generate the power because of its non-pollution and renewable advantage. During the operation, the rotor blades rotate and pass in front of the supporting tower, which causes the blade-tower interaction. This blade-tower interaction can cause problems for wind turbine relating to the unsteady forces leading to structural dynamical loads, unsteady power output, the decrease of the average power output, and the increase of the wind turbine noise and so on (Ansley, 2002; Gipe, 2004; van de berg, 2004; Pedersen, 2003). The main reason is the change of the flow incidence angle when the blade is approaching and leaving the tower. Therefore, it would be useful to consider the blade-tower interaction for the sake of the stable power output and structural stability. Although this problem is known, there is not much research done on this field which will be mentioned on Chapter 2.

In order to reduce the blade-tower interaction, it is necessary to predict this interaction by computer simulation which is less time and cost consuming compared with the experimental method. Based on this, the suitable method for reducing this interaction can be developed. In this thesis, it is aimed at simulating the blade-tower interaction in 2D simulations and correspondingly investigating the feasibility of controlling the unsteady interaction by adaptively pitching blade.

The MB3D CFD code is adopted to simulate the wind turbine blade-tower interaction. The detailed methodology will be descried in Chapter 3. Through the

simulation, the force changing on the blade due to the different blade-tower location in each revolution can be analysed. Based on the result from this simulation, different blade pitching regulation can be analysed and the pitching blade can be also simulated. The amount of this change can be adjusted by changing the pitching degree. Finally, the pitching effect on the blade-tower interaction can be gained through the simulation which will be described at details in Chapter 5.

1.4 Overview of the Thesis

This thesis is aimed at using CFD method MB3D code to compute two turbomachinery unsteady aerodynamic problems, a) fan tone noise transmission cut-on & cut-off situation and b) control the wind turbine blade-tower interaction by adaptive pitching.

In Chapter 1, the CFD application on the turbomachinery unsteady flow is described; also the methods which will be applied on the sound wave transmission and wind turbine blade-tower interaction problems are described as well. In Chapter 2, literature on the fan tone noise problems will be reviewed which includes information on the source of the fan noise, the current prediction methods and noise reducing methods. Also the current wind turbine control systems and the CFD applications on wind turbine are reviewed. In Chapter 3, the methodology used in MB3D code is described. In Chapter 4, the fan tone noise cut-off and cut-on frequency theory are studied, and the corresponding cut-off and cut-on different situations are simulated by using MB3D code. In Chapter 5, the wind turbine blade-tower interactions are simulated and analysed. Subsequently the pitching blade method for minimizing blade-tower interaction is introduced and the pitching effect is simulated. Conclusions from the research are drawn in Chapter 6, with some recommendations for the future work.

CHAPTER 2. LITERATURE REVIEW

2.1 Literature Survey for Fan Noise

2.1.1 Introduction to Fan Noise

Fans are widely used in ventilation systems and air-conditioning systems. Fan noise is consequently a part of global noise, which affects people's life. Even in the office, fan noises are generated not only from the air-conditioning system for the office space, but also from the computer.

Figure 2.1 Ventilation Fan

There are mainly three kinds of factors which affect the fan noise:

(a) The geometric parameters of the fan, which include the diameter, the number of blade and the hub-tip ratio (the ratio of the hub radius to the tip radius). Through a numerical calculation and experiment of the effect of the number of blades on the sound pressure, it is shown that with the number of the blades increasing, the sound pressure level at BPF (blade passing frequency) increases (Jeon, 2002). Also, when the diameter of the impeller is increased, the performance and the fan noise will be increased as well (Heller, 1999).

(b) The immediate environment of the fan, which includes the duct of the fan, the shaped inlet, rotor-stator distance, and the position in the whole ventilation system etc. A better shaped duct inlet can decrease the effect of the upstream distortion by regulating the flow at the machine entry. The level of the acoustic pressure is strongly attenuated when the inlet flow is homogenized, and this decline concerns both the noise at the discrete frequencies (tone noise) and the broadband noise (Maaloum, Kouidri, 2003). The distance between the rotor and stator also affects the fan noise which comes from the rotor-stator interaction. The inlet flow situation is also influenced by the position the fan in the whole system. If the ventilation fans are installed in the straight duct, far away the corner of the duct, the inlet flow can be homogenized thus the fan broadband noise can be decreased.

(c) Fan operation conditions which include the rotational speed and the flow rate. From the acoustic similarity law and the measured data, it is known that the acoustic pressure is proportional to $U^{2.8}$; here U is the blade tip velocity (Weidemann, 1971). Thus, we know that the sound pressure level (*SPL*) will increase with the increase of the rotating speed. If the flow rate is under the off-design condition, the fan noise can be increased whatever the real flow rate is above or below the design flow rate. "The general fan sound law shows that the change of the flow rate coefficient from 0.112 to 0.14 results

in a change of noise by about 0.5dB." (Jeon, 2002). If the flow rate is reduced, the flow pattern is changed such that the flow is separated at the leading edge of the blade and the broadband noise increases.

2.1.2 The Source of Fan Noise

Fan noise is produced by a number of different sources. "Most of the sources involve the interaction of small unsteady flow perturbations with the rotor and the stator blade rows within the stage. These include the interaction of inflow distortions, the inlet boundary layer with the fan, and the interaction of fan flow perturbations (blade viscous wakes, tip clearance flow and so on) with the bypass and the core stators." (Rumsey, 1998; Sato, 1999; Smith, 1997; Envia, Wilson, 2004; Ventres, 1982; Wong, 2003). Depending on the nature of the unsteady perturbations, the interaction sources generate discrete frequency tones (tone noise) and broadband noise which are the mainly noise simulated currently. For subsonic fans, the acoustic tones are usually 10-15dB above the broadband level and mainly due to wake interaction between rotor and stator (Polacsek, Desbois-Lavergne, 2002). Thus, to control and reduce the tone noise is the main task currently. In this thesis, it is aimed at fan tone noise study. Fan tone noise is mainly caused by the periodical perturbations from the rotating blades and the interaction between the rotor and stator. A propagation theory for an idealised 2D duct will be described in Chapter 4.

2.1.3 Typical Ways to Measure and Reduce Fan Noise Level

There are some standards for the fan testing. The European standard ISO 5801 and ISO 5136 govern the aerodynamic and acoustic tests of free inlet fan. Digital micro-manometers, microphone probes and ICP preamplifiers are generally used

in the testing system. When a fan was operated, the noise meter can be used to measure the noise level (Maaloum, Kouidri, 2003).

Current solutions to reduce the fan noise at the source consist of selecting the number of the rotor blades and the number of the stator blades combinations to ensure that the interaction modes at the blade passing frequency (BPF) are cut off. Also, the fan noise can be controlled through adjusting the distance between the rotor and stator to decrease the number and the intensity of the propagating interaction modes. Nowadays, this method is becoming less effective because of the increasing bypass ratios of turban fan engines. Some authors also use a wake generator to reduce the fan interaction noise (Polacsek, Desbois-Lavergne, 2002).

After a fan is designed and manufactured, if it is found to be too noisy, then, some measures can be adopted such as homogenizing the flow at the inlet of the fan; put the fan far away from the curved duct in the system; load the muffle in the exit of the fan; operating in the vicinity of the design point of the machine; reducing the rotational speed without interfering with aerodynamic performances; increasing the rotor-stator distances (Maaloum, Kouidri, 2003). It should be noted that, for a fan with an optimized design from an aerodynamic point of view, the improvement of their acoustic performances may become difficult.

2.1.4 Prediction of Fan Noise Using CAA Method

In addition to the analytical and experimental methods as mentioned above, Computational Aero Acoustics (CAA) has been used to study fundamental aspects of noise generation and propagation in a number of model problems of technical interest like jets, cavity flows, and duct radiation (Freund, Lele, and Moin, 1998; Shieh and Morris, 1999; Goldstein, 1976; Larsson, 2002). The promise of CAA is its ability to simulate accurately the physical processes

involved in the generation and propagation of aerodynamic sound, therefore, it can complement the knowledge gained from analytical and experimental methods. Use of CAA to deal with the fan noise modelling problem has not been fully developed due to the complexity.

This thesis is aimed at analysing the fan tone noise transmission problems; a CFD method is applied to analyse and simulate this aero-acoustic problem which will be described in Chapter 4.

2.2 Literature Review of Wind Turbine

2.2.1 Introduction of Wind Turbine

Wind energy is increasingly used in many countries for generating the power, not only because it is no-pollution, but also because it is renewable energy. European countries such as Holland, Norway and France have been the world leaders in the design and manufacture of wind turbines due to their historical experience of several centuries in building complex wind mill structures, which were used in water pumping, grain grinding and for lumbering (Ansley, 2002; Hansen, 2000).

A wind turbine is a machine to convert the kinetic energy of the wind into the mechanical energy. The mechanical energy can be converted into electricity for daily life or industrial applications. There are two types of wind turbines, which are horizontal axis wind turbine (HAWT) and vertical axis wind turbine (VAWT).

Figure 2.2 HAWT   Figure 2.3 VAWT

Generally, the HAWT is used more than VAWT. For the VAWT, lower energy extraction efficiency is gained than the HAWT because of more turbulent air flow near the ground. And it is difficult to mount the vertical axis turbines on the towers. For the HAWT, the gearbox is on the top of the tower, which includes the yaw mechanism, the electrical switch boxes and control system (Muljadi, Butterfield, 1997).

Typical modern wind turbines have diameters of 40 to 90 meters; towers range from 25 to 80 meters high; most machines operate at a constant speed of 15-50 revolutions per minute, though new designs have variable speed. Almost all wind turbines start operating at a wind speed of 4-5 meters per second and reach maximum power at about 15 meters per second (Muljadi, Butterfield, 1997). Figure 2.4 shows a power curve for a typical Danish 600 KW wind turbine. From the power curve, we can see that when the wind speed is 15 m/s, the power output reaches its maximum. Wind turbines are therefore generally designed so that they yield maximum output at wind speed around 15 meters per second.

Figure 2.4 Power Curve

(http://www.windpower.org/en/tour/wres/pwr.htm)
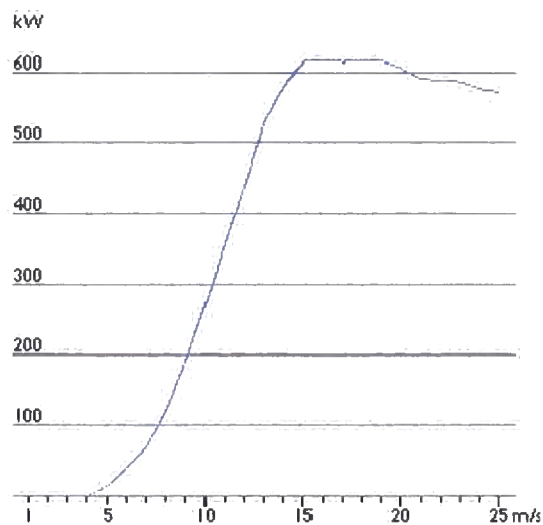
There are some issues of wind turbine. One of them is the noise which includes the mechanical noise and aerodynamic noise. In modern wind turbines, manufacturers have managed to reduce almost all kinds of mechanical noise and are now working on reducing aerodynamic noise from the rotating blades (Hansen, 2000).

The blade-tower interaction is one of the sources which generate aerodynamic noise. Also, the interaction contributes to the blade vibration problem causing blade short life span and wind turbine instability (Pedersen & Halmstad, 2003). Therefore, to minimize the blade-tower interaction will help to reduce the wind turbine noise, increase the blade fatigue life span and improve wind turbine structure stability. A novel method for minimization of the blade-tower interaction is put forward in Chapter 5.

2.2.2 Wind Turbine Control System

All wind turbines are designed with some sort of power control in order to get relative stable power output and avoid damaging itself when the wind is very

strong. There are mainly three different ways of doing this on modern wind turbines, which is stall control, pitch control and yaw control.

- Stall control: Stall controlled wind turbines use a simpler form of blades that are attached to the hub at a fixed angle. The geometry of the rotor blade profile has been aerodynamically designed to ensure that when the wind speed becomes too high, the flow separates from the suction surface and the blade lift starts to fall. This stall prevents a further increase of blade force and hence limits the blade load at a high wind condition. Two thirds of installed wind turbines are stall controlled (Muljadi, Pierce, Migliore, 1998).

- Pitch control: The conventional pitch control system is to pitch the rotor blades slightly out of the wind when the power output becomes too high and will turn the blade back into the wind when the wind drops again according to the electronic controller. On a pitch controlled wind turbine, the actuating mechanism will generally pitch the blades a few degrees every time the wind changes in order to keep the rotor blades at the optimum angle of attack in order to maximize output for all wind speeds. This pitch control system just pitches the blade according to the different wind speeds (Muljadi, Butterfield, 1997). However even though the wind speed is constant, the power is not constant because of the blade-tower interaction. If the blade-tower interaction can be minimized by using a blade pitching, then it does not only benefit to the power output, but also contribute to the wind turbine structure mechanical integrity. The feasibility will be studied in the present work as described in the next chapter.

- Yaw control: An idealized situation for HAWT is that the wind direction is normal to the turbine plane. When the wind direction changes, the turbine plane will change its orientation to match. This is done by a yaw control system, which is constantly trying to rotate the nacelle to minimize the yaw

14

misalignment in order to get as much air through the rotor plane as possible (Farret, Pfischer, Bernardor, 2000).

2.2.3 CFD Applications on Wind Turbine

To increase the output of wind turbines and improve the efficiency and reliability, better understanding of flows around the wind turbine is required. It is difficult to conduct full scale wind tunnel tests because of the size of turbines (a typical blade span is about 10m or more). Schepers at al. (1997) reported their early field tests on a NREL Phase II HAWT blade. Pressure distributions on the blade surface on several spanwise positions are measured. This provides some validation data for CFD codes; however, it is not enough for fully understanding the flow because the available data is limited. Numerical simulation becomes a very important tool for optimal designing of the shape of the blade and the control system. Kang (2001) and Duque et al. (1999, 2000) reported their Navier-Stokes simulation results of the NREL turbine. In their simulations, a multi-block structured-grid with more than one million grid nodes are used around a single blade. The numerical results show good agreement with the experiment except near hub regions at low wind speed conditions.

Different pitch control methods based on the variable wind speed were studied by various researchers (van der Hooft; van Engelen, 2004; Muljadi; Butterfield, 1997). However, adaptive use of pitching blade to reduce the blade-tower interaction has not been reported. In this thesis, the simulation of pitching blade-tower interaction will be studied by using an unsteady CFD code. MB3D code (He, 2006) will be used to simulate the flow for a wind turbine with periodically pitched blades.

CHAPTER 3. COMPUTATIONAL FLUID DYNAMICS METHOD

MB3D code is a multi-block flow solver in 3 dimensions to compute the fluid flow in turbomachinery developed by He (2006) in Durham University. It can compute the compressible steady flow and unsteady flow caused by inlet and /or outlet distortion and/or blade vibration with the cell-centred finite volume scheme with 4-stage Runge-Kutta time-marching method. In this Chapter, the computational methods adopted in MB3D code will be described.

3.1 Governing Equations and Turbulence Model

- **Governing Equations**

All the computational fluid dynamics is based on the fundamental governing equations which are the laws of conservation. The three laws of conservation are those of Mass, Momentum and Energy. A set of partial differential equations are used to express the Navier-Stokes integral equations in order to approximate the behaviour of the fluid flow within the computational domain. In MB3D code, the cylindrical (x, θ, r---axial, circumferential and radial) coordinates are used for convenience of simulating fluid flows in turbomachines, and also an absolute frame of reference is adopted. For a finite control volume δV with a close surface δA, which moves with velocity u_m, v_m, and w_m, the three-dimensional

unsteady Reynolds averaged Navier-Stokes equations, which represent the conservation of mass, momentum and energy, are given in an integral form as follows (Huang, 2006):

$$\frac{\partial}{\partial t}\iiint_{\delta V}U\,dV + \oiint_{\delta A}\left((F-Uu_m)n_x + (G-Uv_m)n_\theta + (H-Uw_m)n_r\right)\cdot d\overset{\rho}{A}$$

$$= \iiint_{\delta V}S\,dV + \oiint_{\delta A}(V_x n_x + V_\theta n_\theta + V_r n_r)\cdot d\overset{\nu}{A}, \qquad (3.1)$$

where, U is the vector of conservative flow variables; F, G, H are the inviscid flux vectors; Uu_m, Uv_m, and Uw_m derive from the contribution of moving grid due to the blade rotation and vibration; $\overset{\nu}{n}=(n_x,n_\theta,n_r)$ is a unit vector in the outgoing normal direction of the cell surface; S is the inviscid source term to account for the centrifugal effect; V_x, V_θ, V_r are the full viscous terms.

$$U = \begin{pmatrix} \rho \\ \rho u_x \\ r\rho u_\theta \\ \rho u_r \\ \rho e \end{pmatrix}, \qquad F = \begin{pmatrix} \rho u_x \\ \rho u_x u_x + P \\ r\rho u_\theta u_x \\ \rho u_r u_x \\ (\rho e + P)u_x \end{pmatrix}, \qquad G = \begin{pmatrix} \rho u_\theta \\ \rho u_x u_\theta \\ r(\rho u_\theta u_\theta + P) \\ \rho u_r u_\theta \\ (\rho e + P)u_\theta \end{pmatrix},$$

$$H = \begin{pmatrix} \rho u_r \\ \rho u_x u_r \\ r\rho u_\theta u_r \\ \rho u_r u_r + P \\ (\rho e + P)u_r \end{pmatrix}, \qquad S = \begin{pmatrix} 0 \\ 0 \\ 0 \\ (P + \rho u_\theta^2)/r \\ 0 \end{pmatrix}, \qquad V_x = \begin{pmatrix} 0 \\ \tau_{xx} \\ r\tau_{\theta x} \\ \tau_{rx} \\ u_x\tau_{xx} + u_\theta\tau_{\theta x} + u_r\tau_{rx} - q_x \end{pmatrix},$$

$$V_\theta = \begin{pmatrix} 0 \\ \tau_{x\theta} \\ r\tau_{\theta\theta} \\ \tau_{r\theta} \\ u_x\tau_{x\theta} + u_\theta\tau_{\theta\theta} + u_r\tau_{r\theta} - q_\theta \end{pmatrix}, \qquad V_r = \begin{pmatrix} 0 \\ \tau_{xr} \\ r\tau_{\theta r} \\ \tau_{rr} \\ u_x\tau_{xr} + u_\theta\tau_{\theta r} + u_r\tau_{rr} - q_r \end{pmatrix},$$

where p, ρ, u_x, u_θ, u_r denote the primitive variables which are pressure, density, total energy and velocity components respectively. The viscous stresses are:

$$\tau_{xx} = \mu(\frac{4}{3}\frac{\partial u_x}{\partial x} - \frac{2}{3}(\frac{1}{r}\frac{\partial r u_r}{\partial r} + \frac{1}{r}\frac{\partial u_\theta}{\partial \theta})), \tag{3.2}$$

$$\tau_{\theta\theta} = \mu(\frac{4}{3}(\frac{1}{2}\frac{\partial u_\theta}{\partial \theta}) - \frac{2}{3}(\frac{\partial u_r}{\partial r} + \frac{\partial u_x}{\partial x})), \tag{3.3}$$

$$\tau_{rr} = \mu(\frac{4}{3}\frac{\partial u_r}{\partial r} - \frac{2}{3}(\frac{1}{r}\frac{\partial u_\theta}{\partial \theta}\frac{\partial u_x}{\partial x} + \frac{u_r}{r})), \tag{3.4}$$

$$\tau_{x\theta} = \tau_{\theta x} = \mu\left(\frac{\partial u_\theta}{\partial x} + \frac{1}{r}\frac{\partial u_x}{\partial \theta}\right), \tag{3.5}$$

$$\tau_{xr} = \tau_{rx} = \mu(\frac{\partial u_r}{\partial x} + \frac{\partial u_x}{\partial r}), \tag{3.6}$$

$$\tau_{\theta r} = \tau_{r\theta} = \mu(\frac{1}{r}\frac{\partial u_r}{\partial \theta} + r\frac{\partial}{\partial r}(\frac{u_\theta}{r})), \tag{3.7}$$

The heat fluxes which arise from the temperature gradients are obtained from the Fourier's heat conduction law:

$$q_x = -k\frac{\partial T}{\partial x}; \qquad q_\theta = -k\frac{\partial T}{r\partial \theta}; \qquad q_r = -k\frac{\partial T}{\partial r}.$$

The system equations are closed by the equation of state:

$$P = (\gamma - 1)\rho(e - \frac{1}{2}(u_x^2 + u_\theta^2 + u_r^2)), \tag{3.8}$$

where k is the molecular thermal conductivity. For the laminar flow, the viscosity μ and thermal conductivity k can be obtained by the Sutherland's law. For the turbulent flow, the molecular viscosity μ and the molecular thermal conductivity k can be expressed as the following equations:

$$u = u_l + u_t, \tag{3.9}$$

$$k = c_p(\frac{\mu_l}{Pr_l} + \frac{\mu_t}{Pr_t}), \tag{3.10}$$

where the subscripts l and t denote laminar and turbulent states respectively. In

(3.10), $Pr_l = \frac{\mu_l c_p}{k_l}$ and $Pr_t = \frac{\mu_t c_p}{k_t}$. The laminar viscosity u_l is obtained from the

18

Sutherland's law with a reference viscosity coefficient being calculated from a fixed Reynolds number at the inlet flow condition; the turbulence viscosity u_t is worked out according to different turbulence model.

- **Turbulence Model**

There are many types of methods to deal with the turbulence, ranging from the simplest algebraic model to the more accurate Large Eddy Simulation (LES) and Direct Numerical Simulation (DNS). Although the LES and DNS methods are more accurate than others, they require prohibitive amount of computing power. In MB3D code, there are two turbulence models which can be chosen to apply. One is the Baldwin-Lomax algebraic mixing length model (Baldwin and Lomax, 1978); the other is the One-Equation Spalart-Allmaras model. In this thesis, when we analyse and simulate the problems, the One-Equation Spalart-Allmaras model was adopted. The Spalart-Allmaras model is an eddy viscosity model based on a transport equation for the turbulent viscosity. It was inspired from the Baldwin-Barth one equation model (Baldwin and Barth 1991). This model aimed at improves the predictions obtained with algebraic mixing-length models and provides an alternative to two equation models. The formulation and coefficients are defined based on dimensional analysis, Galilean invariance, and some selected empirical results. The empirical results used in its development are two-dimensional mixing layers, wakes, and flat-plate boundary layer flows (Zheng, 2004). In the Spalart-Allmaras model (Spalart and Allmaras, 1992), the eddy viscosity function is defined in terms of an eddy viscosity variable, $\tilde{v}$, and a wall function, f_{v1}, as following:

$$v_t = \tilde{v}f_{v1},\tag{3.11}$$

In zones far from wall, the wall function equals to 1.

The convective transport equation of the eddy viscosity is modelled as:

$$\frac{\partial \rho \tilde{v}}{\partial t} + \frac{\partial \rho u \tilde{v}}{\partial x} + \frac{\partial \rho v \tilde{v}}{\partial y} + \frac{\partial \rho w \tilde{v}}{\partial z} = C_{b1}(1 - f_{trip2})\rho \tilde{S}\tilde{v} +$$

$$\frac{1}{\sigma}\left[\begin{array}{c} \dfrac{\partial}{\partial x}\left(\rho(v+\tilde{v})\dfrac{\partial \tilde{v}}{\partial x}\right) + \dfrac{\partial}{\partial y}\left(\rho(v+\tilde{v})\dfrac{\partial \tilde{v}}{\partial y}\right) + \dfrac{\partial}{\partial z}(\rho(v+\tilde{v})\dfrac{\partial \tilde{v}}{\partial z}) + \\ C_{b2}\rho\left(\dfrac{\partial \tilde{v}}{\partial x}\dfrac{\partial \tilde{v}}{\partial x} + \dfrac{\partial \tilde{v}}{\partial y}\dfrac{\partial \tilde{v}}{\partial y} + \dfrac{\partial \tilde{v}}{\partial z}\dfrac{\partial \tilde{v}}{\partial z}\right) \end{array} \right], \qquad (3.12)$$

$$-\left(C_{w1}f_w - \frac{c_{b1}}{\kappa^2}f_{trip2}\right)\rho\left(\frac{\tilde{v}}{d}\right)^2 + f_{trip1}\rho\Delta U^2$$

where the right-hand-side terms represent the turbulence eddy viscosity production, conservative diffusion, non-conservative diffusion near wall turbulence destruction, transition damping of production, and transition source of turbulence. The subscript b stands for "basic", w stands for "wall", and v stands for "viscous".

The basic model constants for free-shear flows to control the production and diffusion of turbulent eddy viscosity are:

$$C_{b1} = 0.1355, \qquad C_{b2} = 0.622, \qquad \sigma = \frac{2}{3}.$$

The additional model constants and auxiliary functions for destruction of turbulent eddy viscosity in the boundary layer are:

$$C_{w1} = C_{b1}/\kappa^2 + (1 + C_{b2})/\sigma, \qquad r = \frac{\tilde{v}}{\tilde{S}\kappa^2 d^2}, \qquad C_{w2} = 0.3,$$

$$g = r + C_{w2}(r^6 - r), \qquad f_w = g\left(\frac{1 + C_{w3}^6}{g^6 + C_{w3}^6}\right)^{1/6}, \qquad C_{w3} = 2.$$

The auxiliary functions for near wall regions are given as:

$$\tilde{S} = S + \frac{\tilde{v}}{(\kappa d)^2}f_{v2}, \qquad S = \sqrt{2S_{ij}S_{ij}}, \qquad \chi = \frac{\tilde{v}}{v}.$$

$$f_{v1} = \frac{\chi^3}{\chi^3 + C_{v1}^3}, \qquad f_{v2} = 1 - \frac{\chi}{1 + \chi f_{v1}}, \qquad C_{v1} = 7.1.$$

The auxiliary functions to control the laminar region of the shear layers and transition to turbulence are defined as:

$$f_{trip1} = C_{trip1}g_{trip} \cdot \exp\left(-C_{trip2}\frac{\omega_{trip}^2}{\Delta U^2}\left(d^2 + \left(g_{trip}d_{trip}\right)^2\right)\right),$$

$$f_{trip2} = C_{trip3} \cdot \exp\left(-C_{trip4}\chi^2\right),$$

$$g_{trip} = \min\left(0.1, \Delta U / \left(\omega_{trip}\Delta x_{trip}\right)\right),$$

$$C_{trip1} = 1.0, \quad C_{trip2} = 2.0, \quad C_{trip3} = 1.2, \quad C_{trip4} = 0.5.$$

where ω_{trip} is the vorticity at the boundary trip point, ΔU is the norm of difference between velocity at a field point and the velocity at the trip point, Δx_{trip} is the grid spacing along the wall at the trip, and d is the distance from the wall.

Boundary conditions must be supplied for the turbulent model. Ideally, when the mesh near the wall is fine enough, the eddy viscosity on solid wall should be set to zero. In most high Reynolds number flow cases, a wall function has to be used in near wall regions to provide enough resolution. For the inlet far from wall and without incoming distortion, the eddy viscosity should be set to zero too, but for numerical reasons, a very small value of the dependent variable ($\tilde{v} < 10^{-6}$) should be used as the inlet condition (Spalart and Allmaras, 1992), which implies a very small value for the eddy viscosity. For an outlet, a simple extrapolation is used to transport information from the computational domain to outside.

3.2 Modes of Flow Solvers

In MB3D code, there are two computational modes for unsteady flows. One is in the frequency domain, and the other is in the time domain.

- **Frequency Domain Solution**

In the frequency domain time-linearised method, it is assumed that the unsteady flow is composed of a perturbation to the steady flow. Furthermore, the perturbation is assumed to be very small so that nonlinear effects can be neglected. In general, nonlinear flow disturbances in time and/or space can be identified and represented by a discrete Fourier series as long as they are periodic. For most engineering applications, only a few lower-order harmonics will be sufficient. Based on this, He (1996) first proposed a novel computational model---the nonlinear harmonic method which has made considerable progress by including the elements of the nonlinear effects. In this method, the flow is taken as an unsteady perturbation to a time-averaged flow rather than a steady flow used in time-linearised methods. In MB3D code, He has developed this method to apply in the rotor-stator blade row aerodynamic interactions, inlet distortions, and aeroacoustic propagations in ducted fans.

- **Time Domain Solution**

The nonlinear time domain method provides more comprehensive physical modelling capabilities to simulate the unsteady flow phenomenon in turbomachines. In this thesis, this time domain method in MB3D was used to simulate and predict the fan tone noise and wind turbine blade-tower interaction.

Time-marching method is a revolutionary invention by Moretti and Abbett (1966) for the solution of transonic flow problems. Since then, a huge variety of numerical schemes based on the time-marching concept have been developed for solving steady transonic inviscid and viscous external and internal flows as reviewed by Ning (1998). The time-marching method has been able to be used for unsteady flow calculation from its birth. As its name suggests, it is the most straightforward method, which time marches the flow state from one instant to the next, and finally to a converged state in which flow shows a 'steady-state' periodically. In the unsteady time-marching calculation, the time domain has a

real meaning. For a periodic unsteady flow, such as the unsteady flow induced by rotor-stator interaction or blade vibration, the final solution must be stepped through many cycles of the transient solution until a steady periodic solution is reached.

There are two different time-marching schemes which are explicit time-marching and implicit time-marching. In the explicit time-marching scheme, the stability of the result is determined by the *CFL* (Courant-Friedrich-Levy) number. If *CFL*<1, the result is convergent and global solution is stable; if *CFL*>1, the solution becomes unstable, the convergent result can't be gained. In the implicit time-marching scheme, the convergent solution always can be gained due to the decay errors. Although there is a potential instability in the explicit time-marching method, this method is always chosen because of the faster computation time. In MB3D code, the explicit time-marching method was adopted.

The major advantage of the time-marching method is the modelling non-linearities. However, it has been recognized that running a time-domain method is time consuming. To speed up time-marching in unsteady calculations, the multi-grid method is developed in the MB3D code (Huang, 2006). The time-consistent multi-grid method was chosen when the wind turbine blade-tower interaction is simulated. In the time-consistent multi-grid method, a uniform global time-step length Δt is usually chosen to be about 20-30 times bigger than the time step $\Delta t'$ determined by the numerical stability (*CFL*) condition. The simplest time-consistent multi-grid is to use just two level grids. In order to improve the accuracy, the intermediate meshes between the fine and coarse mesh are introduced:

$$\delta U_f = \Delta t_f \frac{R_f}{\Delta V_f} + \sum_{i=1}^{M} \Delta t_i \frac{R_i}{\Delta V_i} + \Delta t_c \frac{R_c}{\Delta V_c} \qquad (3.13)$$

where R stands for the flow equation residual value, the subscripts f, i and c denote the fine mesh, the ith intermediate mesh (of M levels) and the coarse mesh

respectively. Δt_f and Δt_i are the allowable time-step lengths on the fine mesh and the ith intermediate mesh respectively. For unsteady calculations, the uniform time-step length Δt is maintained throughout the computational domain by selecting the coarse block step-size Δt_c to satisfy:

$$\Delta t_c = \Delta t - \Delta t_f - \sum_{i=1}^{m} \Delta t_i \qquad (3.14)$$

3.3 Finite Volume Time-marching Scheme

In the MB3D code, the governing equations are discretized in space using the cell-centered finite volume scheme and the space-discretized equations are using the second order accurate explicit four-step Runge-Kutta time-marching approach. The equations are the following:

$$U^{n+1/4} = U^n \frac{\Delta V^n}{\Delta V^{n+1/4}} - \frac{1}{4} \frac{\Delta t}{\Delta V^{n+1/4}} \left(R_i^n + R_v^n - D^n \right), \qquad (3.15)$$

$$U^{n+1/3} = U^n \frac{\Delta V^n}{\Delta V^{n+1/3}} - \frac{1}{3} \frac{\Delta t}{\Delta V^{n+1/3}} \left(R_i^{n+1/4} + R_v^n - D^n \right), \qquad (3.16)$$

$$U^{n+1/2} = U^n \frac{\Delta V^n}{\Delta V^{n+1/2}} - \frac{1}{2} \frac{\Delta t}{\Delta V^{n+1/2}} \left(R_i^{n+1/3} + R_v^n - D^n \right). \qquad (3.17)$$

$$U^{n+1} = U^n \frac{\Delta V^n}{\Delta V^{n+1}} - \frac{\Delta t}{\Delta V^{n+1}} \left(R_i^{n+1/2} + R_v^n - D^n \right), \qquad (3.18)$$

Where R_i is the net inviscid fluxes and R_v is the net viscous fluxes through cell surfaces.

$$R_i = \sum \left(\left(F - U u_{mg} \right) \Delta A_x + \left(G - U v_{mg} \right) \Delta A_\theta + \left(H - U w_{mg} \right) \Delta Ar \right) + S \Delta V, \qquad (3.19)$$

$$R_v = \sum \left(V_x A_x + V_\theta A_\theta + V_r A_r \right), \qquad (3.20)$$

To damp numerical oscillations, the artificial dissipation term $D = \sum d$ is introduced. A blend of second-order and fourth-order adaptive smoothing is utilized. In detail at the surface between cell (i, j, k) and cell $(i, j+1, k)$,

$$d_{i,j+\frac{1}{2},k} = \left(\varepsilon^{(2)}_{i,j+\frac{1}{2},k} \left(U_{i,j+1,k} - U_{i,j,k} \right) - \varepsilon^{(4)}_{i,j+\frac{1}{2},k} \left(U_{i,j+2,k} - 3U_{i,j+1,k} + 3U_{i,j,k} - U_{i,j-1,k} \right) \right) \frac{\Delta V_{i,j+1,k}}{\Delta t}$$

(3.21)

where $\varepsilon^{(2)}$ and $\varepsilon^{(4)}$ are second-order and fourth-order smoothing coefficients that are defined as follow:

$$\varepsilon^{(2)}_{i,j+\frac{1}{2},k} = \max\left(v_{i,j+2,k}, v_{i,j+1,k}, v_{i,j,k}, v_{i,j-1,k} \right),$$

(3.22)

$$v_{i,j,k} = K^{(2)} \left| \frac{p_{i,j+1,k} - 2p_{i,j,k} + p_{i,j-1,k}}{p_{i,j+1,k} + 2p_{i,j,k} + p_{i,j-1,k}} \right|,$$

(3.23)

$$\varepsilon^{(4)}_{i,j+\frac{1}{2},k} = \max\left(0, \left(K^{(4)} - K^{(2\&4)} \varepsilon^{(2)}_{i,j+\frac{1}{2},k} \right) \right),$$

(3.24)

where $K^{(2)}$, $K^{(4)}$ and $K^{(2\&4)}$ are constants used to control the amount of numerical dissipation.

3.4 Boundary Condition

A numerical solution of the fluid governing equations can not be completed without boundary conditions being specified. There are several kinds of boundary conditions in MB3D code. In the fan tone noise transmission and wind turbine blade-tower interaction simulation problems, the inlet, outlet, distort, far field, solid wall and periodic boundary conditions are used.

- **Inlet/Outlet Boundary**

For a subsonic flow as analysed in this thesis, at the inlet boundary, total pressure, total temperature and the flow angles are specified; at the outlet boundary, the static pressure is specified, and other undefined flow variables at the outlet boundary are extrapolated from the interior of the domain. In order to avoid the non-physical reflections from the inlet and outlet boundaries, a simplified one-dimensional non-reflecting boundary treatment (Giles, 1990) is

applied in MB3D, which reduces the length of the inlet and outlet computational domains; therefore the computation time is saved.

- **Distort on the Inlet/Outlet Boundary**

When there are disturbances in the inlet or outlet boundary, these disturbances are assumed to be periodic temporally and spatially in the MB3D code, and the flow variables U can be decomposed into a time-averaged part $\overline{U}$ and a number of unsteady disturbances u_i identified by their temporal periodicities. Each disturbance can be approximated by a set of Fourier series in time as the follows:

$$U(x,\theta,r,t) = \overline{U}(x,\theta,r) + \sum_{i=1}^{N_{pt}} u_i(x,\theta,r,t), \tag{3.25}$$

$$u_i(x,\theta,r,t) = \sum_{n=1}^{N_{fou}} \left(A_{n,i} \sin(n(\omega_i t + \sigma_i)) + B_{n,i} \cos(n(\omega_i t + \sigma_i)) \right), \tag{3.26}$$

where, N_{pt} is the number of disturbances; ω_i is the fundamental frequency of the ith unsteady disturbance; $A_{n,i}$ and $B_{n,i}$ are the corresponding Fourier coefficients; N_{fou} is the order of the Fourier series; x, θ, and r are axial, circumferential and radial coordinates respectively; t is the physical time; σ_i is the inter-blade phase angle.

In the fan tone noise simulation, the outlet disturbance will be applied.

- **Far Field**

In external aerodynamics, the flow has relatively uniform free-stream conditions far from the body. In numerical simulations, flow domains have to be truncated to a finite distance from the body. These truncated faces are known as far field boundaries. In this boundary condition, the stagnation pressure, the stagnation temperature, the velocity and the flow angle are input which will in turn give the far field velocity and pressure. These will be used to specify any incoming flow

characteristics for applying boundary conditions according to the local mesh orientation. In the wind turbine blade-tower simulation, this kind of boundary condition is adopted which will be described in Chapter 5.

- **Solid Wall Boundary**

At solid walls, the mesh grid points on solid wall surfaces are moving to comply with the blade rotation and/or vibration. For the non-slip wall boundary condition, because the viscous layers are very thin, the mesh near the wall surface must be very refined, which will cause additional computational cost due to the mesh refinement. Thus, fluid at the solid boundary is allowed to slip and an approximate log-law model (Denton, 1992) was applied in order to compute the wall shear stresses in the MB3D code:

$$\frac{\tau_w}{0.5\rho_w \mu_w^2} = -0.001767 + \frac{0.03177}{\ln(\mathrm{Re}_w)} + \frac{0.25614}{(\ln(\mathrm{Re}_w))^2}, \tag{3.27}$$

where u_w and ρ_w are velocity and density at the first grid point away from the solid surfaces and $\mathrm{Re}_w = \rho_w u_w \Delta n / \mu$. Comparing to the non-slip condition, this slip wall condition allows coarser mesh in the near wall region.

- **Periodic Boundary**

A periodic boundary is present in most turbomachinery applications. For a mesh with a periodic condition, periodic nodes and edges are treated as inner nodes and edges, the fluxes through the pair of edges are calculated only one time and given to two periodic cells. In the wind turbine blade-tower interaction simulation, the periodic boundary was adopted which will be described in Chapter 5.

CHAPTER 4. ANALYSIS OF FAN TONE NOISE PROPAGATION

4.1 Introduction

In Chapter 2, the source of the fan noise and its affecting factors are reviewed. The basic understanding and useful guidance can be gained by looking into the noise propagation in a simple system. Tyler & Sofrin first put forward the theory of the fan tone noise generation and transmission system in 1962. In this chapter, this theory is described; and the different cut-on and cut-off sound wave transmission situations are correspondingly simulated by using the CFD method.

4.2 Fan Tone Noise Propagation

Once a blade starts to rotate, it will generate noises which came from the pressure fluctuations due to the non-uniform pressure field rotating with the blade. The pressure pattern is generated circumferentially. According to the generating mechanisms and its periodic characteristic, the pressure fluctuations can be expressed by a harmonic series of component frequencies through using the Fourier Transform. The pressure at a fixed radius and axial location can be expressed as:

$$P(\theta,t) = \sum_{n=0}^{\infty} a_n \cos[nB(\theta - \Omega t) + \phi_n],$$ (4.1)

where θ --Angular coordinate, radians;

      t --Time coordinate;

      a_n --Amplitude coefficient;

      ϕ_n --Phase angle;

      n --Harmonic number (n=1 for the fundamental blade passing

        disturbance);

      B --Number of rotor blades;

      Ω --Rotor shaft speed, radians/sec.

For the fixed angular reference position θ =0, the function (4.1) can be simplified as in Eq (4.2) giving the temporal variation. For the temporal reference time, $t = 0$, the function (4.1) can be simplified as shown in Eq (4.3) giving an instantaneous spatial variation. The pressure patterns for a rotor with 4 blades are illustrated through Figure 4.1, 4.2 & 4.3.

$$P(t) = \sum_{n=0}^{\infty} a_n \cos(nB\Omega t - \phi_n), \qquad (4.2)$$

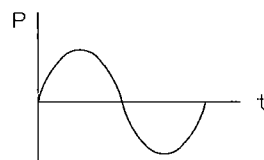$$P(\theta) = \sum_{n=0}^{\infty} a_n \cos(nB\theta + \phi_n), \qquad (4.3)$$

$$\Omega = 2\pi N .$$

(1) For $f = BN$ (fundamental harmonic), B Lobes situation,
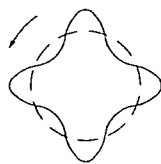
    Spatial Pressure Pattern   Time Trace

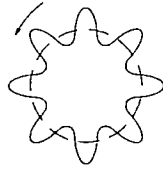 $P_1(\theta) = a_1 \cos(B\theta + \phi_n)$ $P_1(t) = a_1 \cos(B\Omega t - \phi_n)$

Figure 4.1 Pressure Variations in time and space, n=1

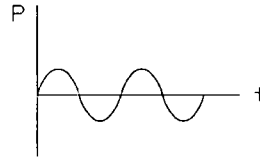(2) For $f = 2B$N (the first harmonic), 2 B Lobes situation,

Spatial Pressure Pattern   Time Trace

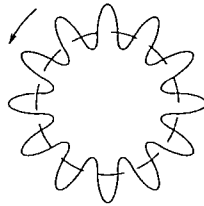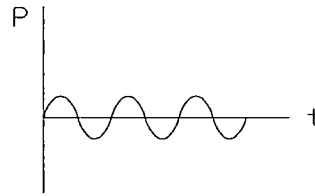$$P_2(\theta) = a_2 \cos(2B\theta + \phi_n)$$ $$P_2(t) = a_2 \cos(2B\Omega t - \phi_n)$$

Figure 4.2 Pressure Variations in time and space, n=2

(3) For $f = 3B$N (the second harmonic), 3 B Lobes situation,

Spatial Pressure Pattern   Time Trace

$$P_3(\theta) = a_3 \cos(3B\theta + \phi_n)$$ $$P_3(t) = a_3 \cos(3B\Omega t - \phi_n)$$

Figure 4.3 Pressure Variations in time and space, n=3

As we know, the flow passage in an axial flow fan is bounded by the casing wall outside and hub inside. Thus, the propagation of pressure waves is bounded by these two concentric cylinders. In the reference plane near the rotor, the pressure distribution can be represented by the following function:

$$P_m(r,\theta,t) = P_m(r)\cos[m(\theta - \Omega_m t) + \phi_m],$$ (4.4)

where $P_m(r)$--the radial distribution function (Eq (4.5));

m --Number of lobes or cycles of circumferential pressure (here, $m = nB$);

ϕ_m --Phase of m -th mode;

Ω_m --Angular velocity of m -lobe spinning pattern;

Using the Bessel Function, the radial distribution pressure can be expressed as follows:

$$P_m(r) = \sum_{\mu=0}^{\infty} a_{m\mu} P_{\mu}(r) = a_m \sum_{\mu=0}^{\infty} a_{\mu} P_{\mu}(r), \qquad (4.5)$$

where $P_{\mu}(r)$ --E-functions, which depends on m, σ (hub-tip ratio), and μ (the number of nodes in the radial direction);

$a_{m\mu}$ or a_{μ} --weighting coefficients;

Now a parameter $K_{x\mu}$ relating f and $f_{m\mu}$ is introduced:

$$K_{x\mu} = \frac{2\pi}{c} \sqrt{f^2 - f_{m\mu}^2} = \sqrt{\left|\left(\frac{\omega}{c}\right)^2 - \left(\frac{2\pi f_{m\mu}}{c}\right)^2\right|}$$

$$= \sqrt{\left|\left(\frac{m\Omega}{c}\right)^2 - \left(K_{m\mu}^{(\sigma)}\right)^2\right|} = \frac{m}{b}\sqrt{\left|M_m^2 - \left(K_{m\mu}^{\prime(\sigma)}/m\right)^2\right|}, \qquad (4.6)$$

where f --driving frequency which can make the pressure wave transmit circumferentially;

$f_{m\mu}$ --Cut-off frequency of (m, μ) mode; the generated frequency if this wave were supposed to travel in free space with natural velocity c along the circumferential direction;

b --Outer wall radius;

M_m --Circumferential Mach number for m-lobe pattern, $M_m = \dfrac{b\Omega}{c} = \dfrac{c_m}{c}$;

$K_{m\mu}^{(\sigma)}$ --Characteristic number depended on m, μ and σ.

When $M_m \geq K_{m\mu}^{\prime(\sigma)}/m$, the wave can be propagated along the length of duct (x-axial); when $M_m < K_{m\mu}^{\prime(\sigma)}/m$, the wave will decay along the x-axis. According to the thin circular duct transmission, it is noted that the higher cross-nodes are, the higher cut-off frequency obtained. Consequently, the pressure wave will propagate as long as $M_m < M_m^* = K_{m0}^{\prime(\sigma)}/m$, here M_m^* was the critical

circumferential tip Mach number for the lowest radial mode ($\mu = 0$). Accordingly, f_{m0} was called the cut-off frequency.

4.3 Pressure Wave Transmission Characteristics

According to the analysis above, the transmission characteristics can be summed up as below.

(a) Decay situation.

When $f < f_{m0} (M_m < M_m^\bullet)$, the pressure wave will decay along the duct.

The pressure distribution can be expressed as the function below:

$$P(r,\theta,x,t) = a_{m\mu}P_\mu(r)\cos\left[m(\theta - \Omega_m t) + \phi_m\right]e^{-k_{x\mu}x}, \tag{4.7}$$

where $k_{x\mu} = \dfrac{m}{b}\sqrt{\left(k_{m\mu}^{'(\sigma)}\middle/m\right)^2 - M_m^2}$

$$(c_m < c, \lambda_m = \frac{2\pi b}{m} < \lambda)$$

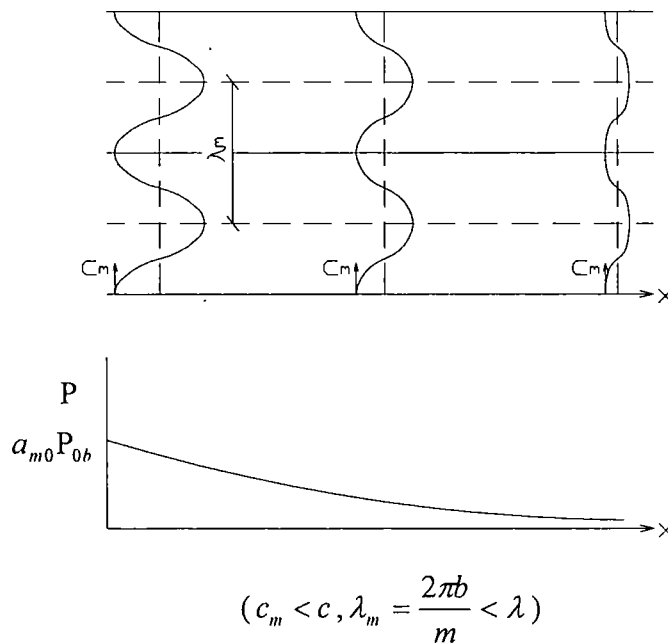Figure 4.4 Properties of Decaying Field

(Outer wall of duct)

Through the Figure 4.4 above, the decay situation can be seen obviously. As long as $f < f_{m0}(M_m < M_m^{\bullet})$, all waves including the modes $\mu > 0$ will decay.
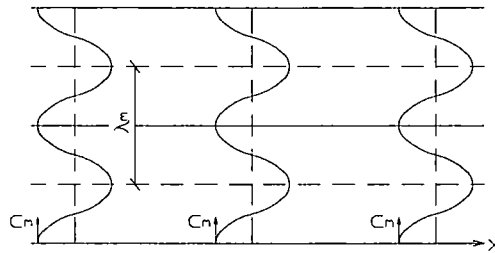
(b) Resonance situation

When $f = f_{m0}(M_m = M_m^{\bullet})$, the pressure wave will be the same along the duct. Under this situation, the pressure distribution can be expressed as the function below:

$$P(r,\theta,x,t) = a_{m0}P_0(r)\cos\left[m(\theta - \Omega_m t) + \phi_m\right] \qquad \text{(For } \mu = 0 \text{ mode)} \qquad (4.8)$$

The pressure field of $\mu > 0$ modes when they are at cut-off is expressed as below:

$$P(r,\theta,x,t) = a_{m\mu}P_\mu(r)\cos\left[m(\theta - \Omega_m t) + \phi_m\right] \qquad \text{(For } \mu > 0 \text{ modes)} \qquad (4.9)$$

$$(c_m = c, \ \lambda_m = \lambda = \frac{2\pi b}{m})$$

Figure 4.5 Properties of Resonance Field

(Outer wall of duct)

From the Figure 4.5 above, it can be seen that the pressure wave is the same along the duct.

(c) Propagation situation

When $f > f_{m0}(M_m > M_m^{\bullet})$, the pressure wave can be propagated along the duct. The pressure field for $(m,0)$ mode is expressed as below:

$$P(r,\theta,x,t) = a_{m0}P_0(r)\cos\left[m(\theta - \Omega_m t) + K_x x + \phi_m\right], \qquad (4.10)$$

where $K_x = \dfrac{m}{b}\sqrt{M_m^2 - \left(M_m^*\right)^2}$

The pressure field for (m,μ) modes when they are at cut-off is expressed as below:

$$P(r,\theta,x,t) = a_{m\mu}P_\mu(r)\cos\left[m(\theta - \Omega_m t) + K_{x\mu}x + \phi_m\right], \qquad (4.11)$$

where $K_{x\mu} = \dfrac{m}{b}\sqrt{M_m^2 - \left(K_{m\mu}'^{(\sigma)}\Big/m\right)^2}$

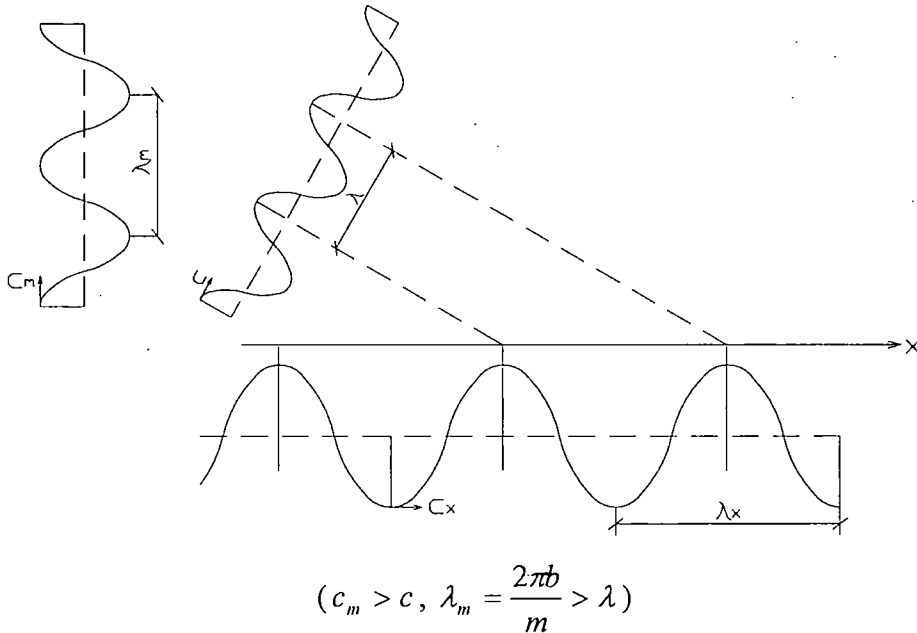
$$(c_m > c, \ \lambda_m = \frac{2\pi b}{m} > \lambda)$$

Figure 4.6 Properties of Propagating Field

(Outer wall of duct)

From Figure 4.6, we can see that when $c_m > c$, the pressure wave starts to propagate along the duct with an inclined angle.

For $\mu > 0$ modes, we know $f_{m\mu} > f_{m0}$. When $f > f_{m\mu}$, then all the $\mu > 0$ modes will propagate.

In fact, the critical circumferential tip Mach number M_m^* always above 1 for different m and σ . The critical tip velocity $M_m^* c$ is always supersonic. However, along the radial direction, the velocity is different because of different radius. Accordingly, there always one point whose Mach number is equal to 1 corresponding to M_m^* at cut off. This point can be called the "center of propagation" which was simplified by using this point sometimes.

The discussion above is based on the rotor only generation mechanism, for the rotor-stator interaction mechanism, the pressure distribution is different from function (4.1). It can be expressed as below:

$$\mathrm{P}(\theta,t)= \sum_{n=1}^{\infty} \sum_{m=-\infty}^{\infty} Va_{mn} \cos\left[m\left(\theta - \frac{nB}{m}\Omega t \right) + \phi_{mn} \right], \qquad (4.12)$$

where $m = nB + kV$, $k = \ldots -2, -1, 0, 1, 2 \ldots$
   V = the number of stator vanes

Although the pressure functions are different in the two different generating mechanisms, the analysis method is the same in relation to the propagation, and forms of the two equations are similar. The different mode number m is applied to get the value of the cut-off frequency.

4.4 Simulation of Sound Wave Transmission in Cut-on and Cut-off Situations

Based on the analysis of the pressure wave transmission theoretically, the decay situation (cut-off situation) and the propagation situation (cut-on situation) can be simulated by using MB3D code. In the simulation of wave pressure

transmission along the duct, a cylinder is used to simulate the narrow annular duct, and the pressure wave transmission along the duct surface circumferentially will be simulated and analysed. At the exit of the duct, the duct is subject to upstream running acoustic waves to simulate a rotating unsteady pressure field which is generated by a fan rotor. In this case, one block is adopted to simulate the cylinder as our whole computational domain. Figure 4.7 shows the computational domain.
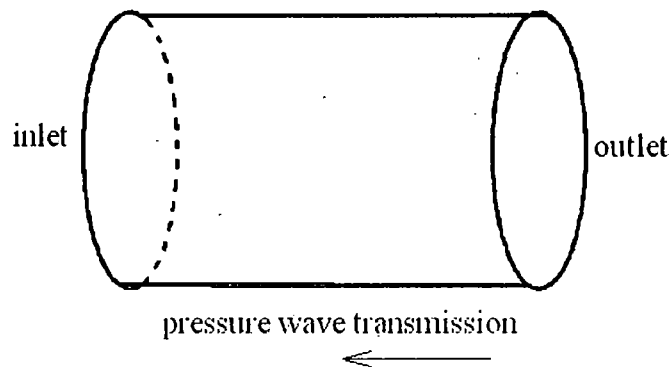

Figure 4.7 Computational Domain for Pressure Wave Transmission

Here, the axial length of the cylinder is taken as 0.5 meter, and the circumferential length of the cylinder is 1 meter. Numerical test showed that for the present second-order spatial discretization, at least 20 mesh points should be needed for accurately resolving one harmonic. In this case, 25 mesh cells per wavelength are applied here. Along the axial length of the cylinder, totally 101 mesh points were adopted; along the circumferential length, totally 201 mesh points were used. Thus, the mesh space is the same in both two directions. The mesh projection in 2D is shown in Figure 4.8 as follows. The pressure disturbances are specified at the exit.
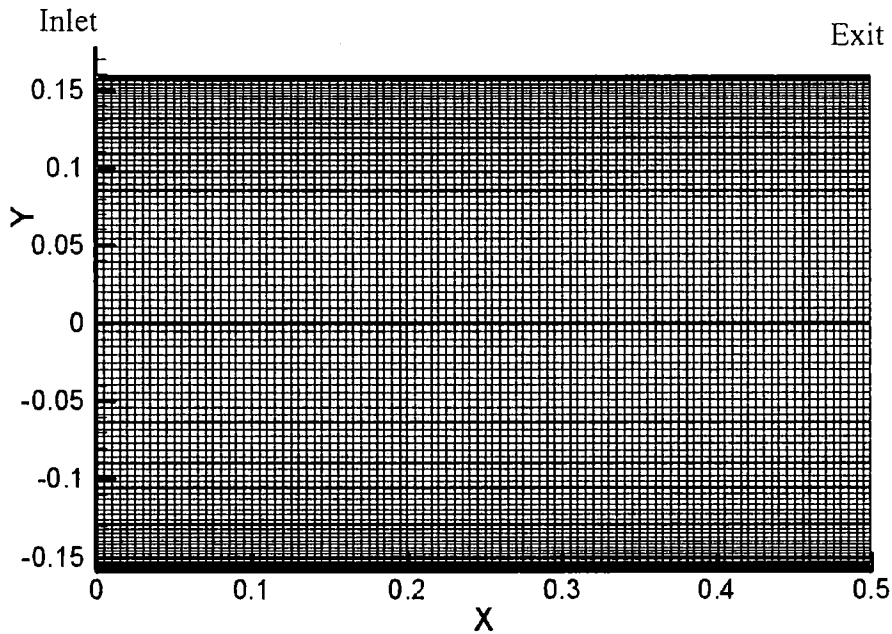
Figure 4.8 The Mesh Projection in 2D

In the inlet of the cylinder, the total pressure is set up as $10^5 Pa$, the total temperature is $298K$, and the flow angle is zero; in the outlet of the cylinder, the static pressure is defined as $0.7 \times 10^5 Pa$. Also, in order to simulate the fan rotor at the outlet of the cylinder, a distortion at the outlet boundary was added. A 0.15% of the total pressure perturbation is set up, and the pressure perturbation is set up as a sinusoidal regulation circumferentially. Non-reflective boundary condition was adopted. By specifying different frequencies for the distortion, different pressure wave transmission situation is simulated as follows.

According to the analysis of the theory of the sound wave, it is noted that when the driving frequency is below the cut-off frequency, the pressure wave will decay along the duct (cut-off situation), and when the driving frequency is above the cut-off frequency, the pressure wave can propagate along the duct without any decay. With different driving frequencies, these cut-on and cut-off situations are simulated by using MB3D code as following below.
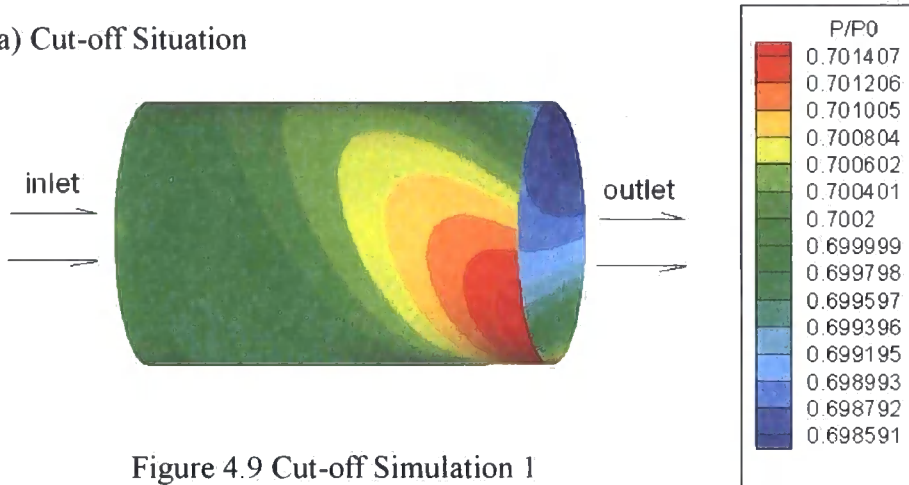
37

(a) Cut-off Situation

Figure 4.9 Cut-off Simulation 1

Figure 4.9 shows the situation of the pressure wave transmission under the condition of the cut-off ratio (driving frequency/cut-off frequency) is 60.6%. From the different values of the static pressure, it can be seen that, in this situation, the pressure wave can not be propagated upstream along the duct; while, with the transmission, it is decayed very quickly. With a different cut-off ratio, the decay rate is different. Figure 4.10 shows another cut-off situation with the cut-off ratio is 30.3%, indicating a faster decay compared with the previous case.
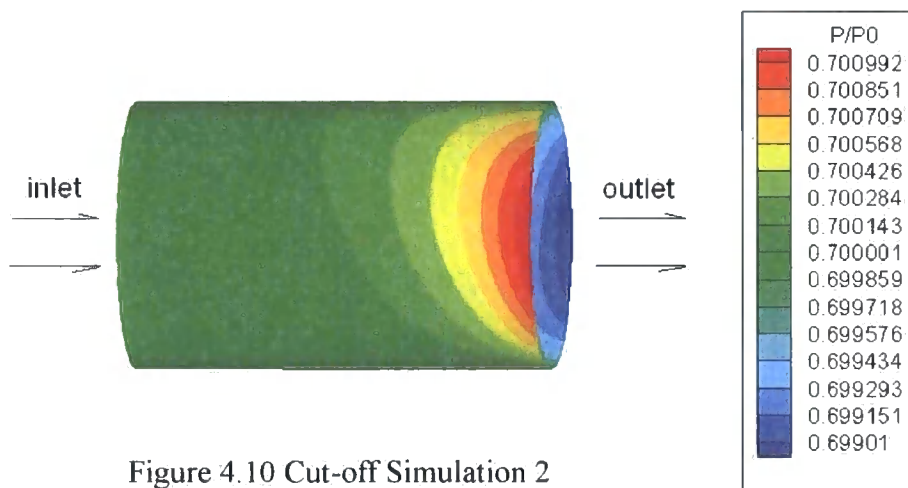

Figure 4.10 Cut-off Simulation 2
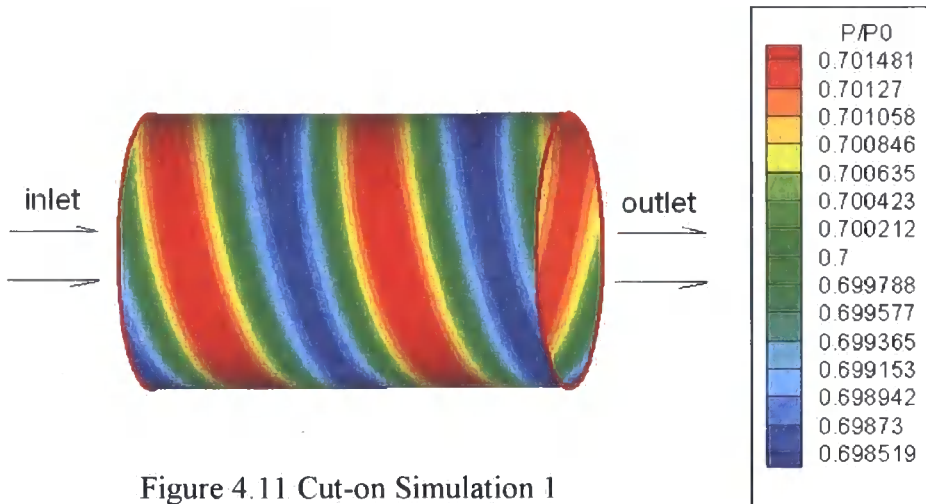
(b) Cut on Situation

Figure 4.11 Cut-on Simulation 1

The cut-on situation is simulated with the increased driving frequency. Figure 4.11 shows the situation of the pressure wave transmission under the condition of the cut-on ratio (driving frequency/cut-off frequency) is 120.2%. From the different values of the static pressure, we can see, in this situation, the pressure wave can propagate upstream along the duct without any decay. Figure 4.12 shows another cut-on situation with a different cut-on ratio 144.0%, indicating a faster propagation compared with the previous case.
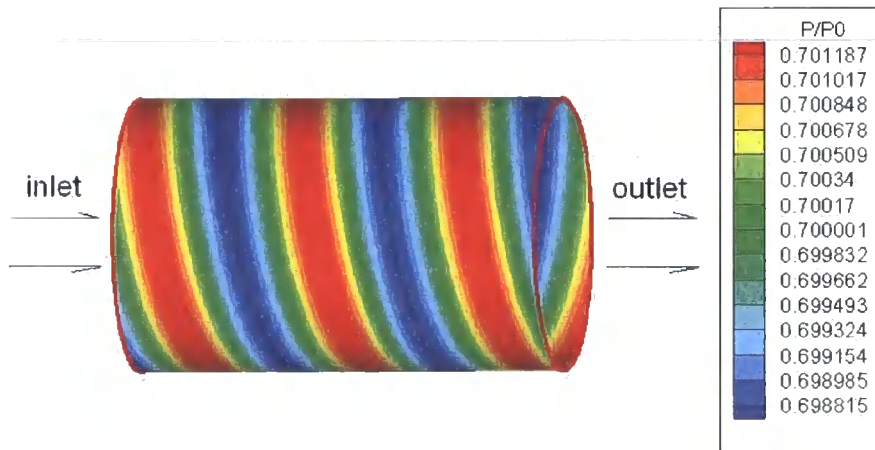

Figure 4.12 Cut-on Simulation 2

4.5 Summary

In this Chapter, the sound wave transmission along the narrow annular duct in the moving media has been studied. With different driving frequencies, the different pressure wave transmissions are simulated by using the CFD MB3D code. Based on the calculation results, when the driving frequency is below the cut-off frequency, the pressure wave will decay along the duct, and the decay rate will increase with the cut-off ratio decreasing. When the driving frequency is above the cut-off frequency, the pressure wave can propagate upstream along the duct without any decay. Unfortunately, since there are no theoretical and experimental results found in the open literature, the simulation results are not compared with the theoretical/experimental results in this thesis.

Usually the acoustic waves have small amplitudes relative to numerical errors. This makes the difficulty to simulate the acoustic wave. The simulation results in this chapter proved that this CFD method can simulate such acoustic waves in 2D situation. Therefore, this method can be developed to apply on the concentric cylindrical duct pressure wave transmission 3D simulation. In 3D, cut-on and cut-off situations can simultaneously occur in different radii, which makes part span cut-on and part span cut-off situation. Moreover, this code can be developed to simulate pressure wave transmission under non-axisymmetric flow.

CHAPTER 5. ANALYSIS OF WIND TURBINE BLADE-TOWER INTERACTION AND PERIODIC PITCHING FOR ACTIVE CONTROL

Based on the literature review of wind turbine in Chapter 2, it is known that wind turbine blade-tower interaction will cause increased dynamic stresses of the blades, rise in the wind turbine noise and unsteady power output. In this Chapter, we will use the CFD MB3D code to simulate the blade-tower interaction and study the feasibility for an adaptive pitching control of the interaction.

5.1 Wind Turbine Blade-Tower Interaction

For a typical HAWT wind turbine, while the blades rotate, the aerodynamic load changes periodically in time because of the blade-tower interaction, and the range of the load is influenced by some factors, such as the distance between the rotor and tower, and the wind speed. This unsteady blade force variation can be simulated by using MB3D code. Figure 5.1 shows the starting relative position of the blade and tower in a 2D situation.
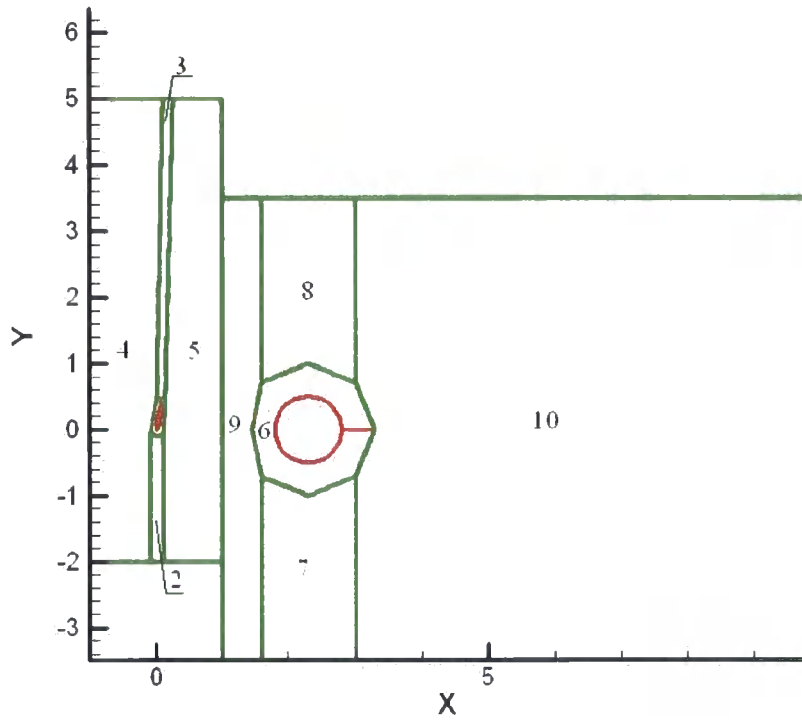
Figure 5.1 One Blade and Tower 2D Domain with Block Indices
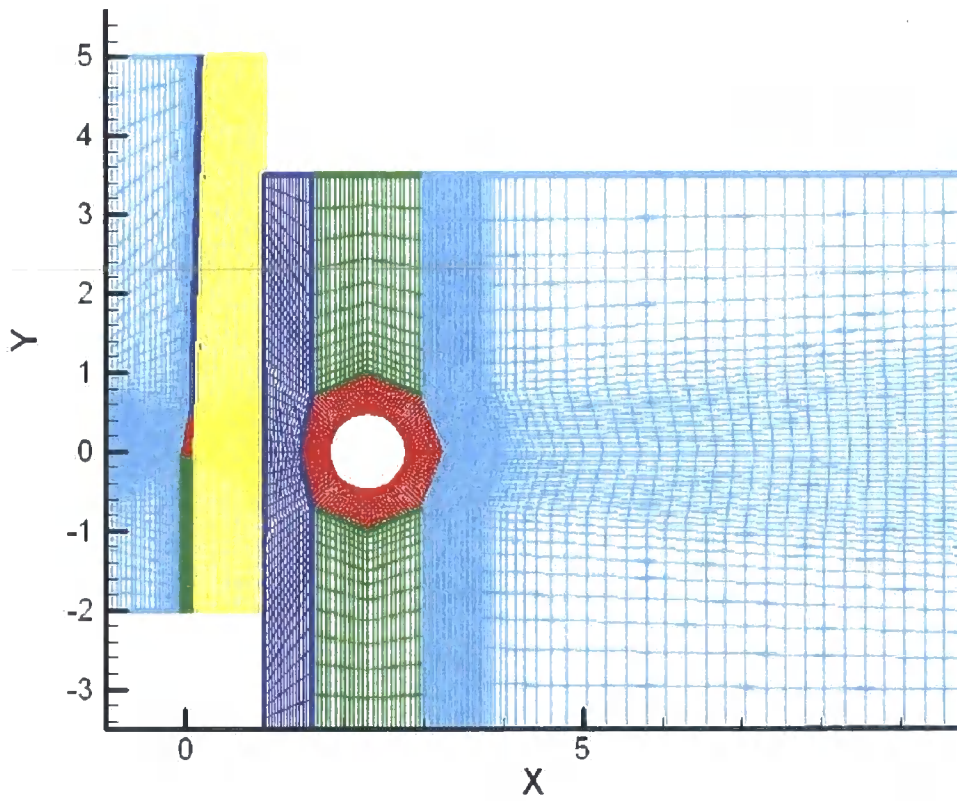

Figure 5.2 One Blade and Tower 2D Mesh

Figure 5.1 and Figure 5.2 shows the blade with tower 2D computational domain. In this simulation, the multi-block structured mesh is used. There are total 10 blocks in this computational domain. The block 1 is around the blade, which is shown in Figure 5.3. The block 6 is around the tower, which is shown in Figure 5.4.
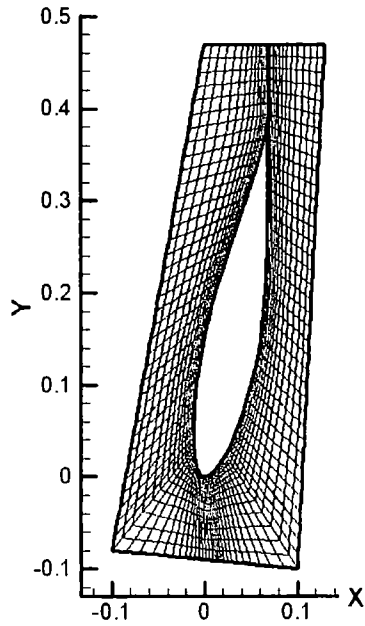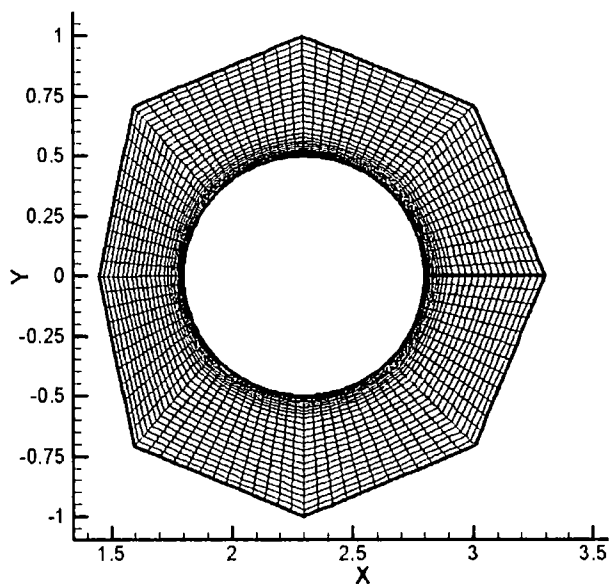

Figure 5.3 Block 1 Mesh

Figure 5.4 Block 6 Mesh

For the left edge of the block 4 and the right edge of the block 10, the far field boundary condition is applied; for the upper edge of blocks 4, 3, 5, 9, 8, 10, and the bottom edge of blocks 4, 2, 5, 9, 7, 10, the periodic boundary condition is applied; for the block 1 and 6, which are around the blade and tower, the solid wall boundary condition is applied. In this simulation, the wind speed is defined to be 15m/s, the diameter of the tower is 1m. From Figure 5.3, it can be measured that the angle between the blade's chord and the x axis is 83.4°; in order to make the flow incidence angle close to zero which is good to the flow areodymamic, the tangential speed of the blade is defined at 1.75m/s. The different situations with different distances between blade and tower are simulated respectively, and the corresponding force variations in x (axial) and y (tangential) two directions are analyzed accordingly.

The different gap distances between the blade (Mid-chord) and the tower (Leading Edge) will cause different force variations on the blade. Two different gap distances are chosen, which are 1.8m and 1.3m in the simulation. As the diameter of the tower is 1m, the gap distances are expressed in terms of the tower diameter as 1.8D and 1.3D. In order to compare the extent of the force variation, the non-dimensional force expression was adopted; the instantaneous force (the "force" in Chapter 5 means the "force acting on the blade") is normalized by the time-averaged value. Figure 5.5 and Figure 5.6 show the non-dimensional force comparisons between the two different gap distances.
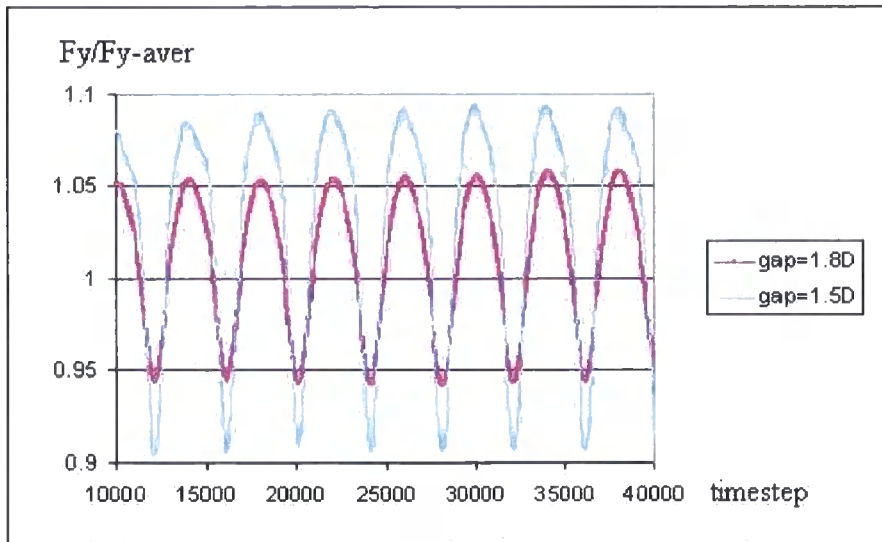
Figure 5.5 Non-Dimensional Force Comparisons in Tangential Direction
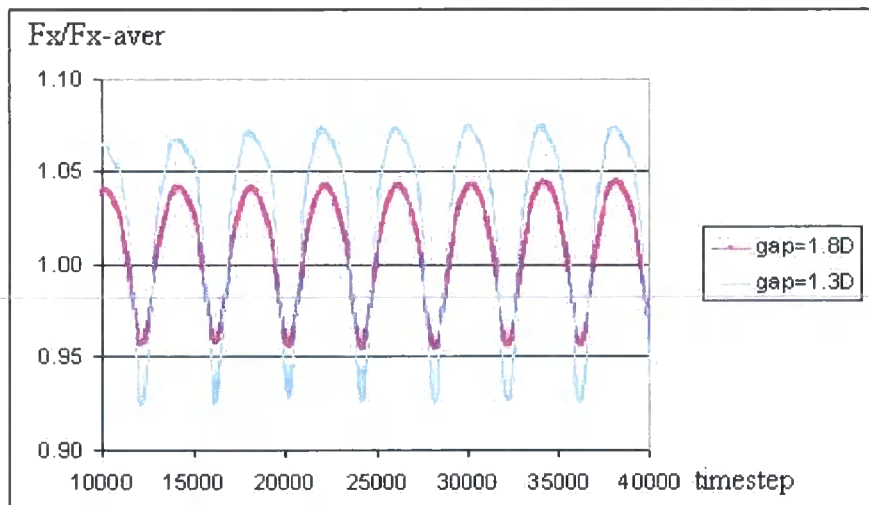

Figure 5.6 Non-Dimensional Force Comparisons in the Axial Direction

From Figure 5.5 and Figure 5.6, it can be seen that the force variations are quite different with the different gap distances between blade and tower. The quantitative comparisons are shown in Table 5.1.

45

Table 5.1 Non-dimensional Force Comparisons with Different Blade-Tower Gap

Force Distance	FY_{min}/FY_{av}	FY_{max}/FY_{av}	Variation percentage	FX_{min}/FX_{av}	FX_{max}/FX_{av}	Variation percentage
Gap=1.8D	0.942	1.058	11.62%	0.955	1.045	9.00%
Gap=1.3D	0.906	1.094	18.78%	0.925	1.075	14.99%

Table 5.1 shows the minimum and maximum values of the non-dimensional force and the variation percentage. When the blade-tower distance is reduced, the force variation is noticeably enlarged. Through increasing the blade-tower gap distance, the force variation can be decreased. However, the blade-tower distance can not be increased too much considering the wind turbine structure balance and the bending momentum. Therefore, it is necessary to consider another possible option to control and reduce this interaction. The question is whether a periodic pitching of blades can be made or not to control the blade-tower interaction actively. This issue is addressed in section 5.2 & 5.3.

5.2 One Blade Adaptive Pitch Simulation for Active Control

The simulation results in section 5.1 show the blade force variation in one revolution. In order to control and reduce the force variation on the blade, further blade force simulations are analyzed in this section. First, the blade force variations caused only by pitching the blade are simulated, and then the pitching blade simulation is added onto the wind turbine rotating blade to predict new force variation after adding this adaptive pitch.

For a pitching blade in isolation, the computational domain is shown in Figure 5.7. In this simulation, the simple sinusoidal pitching displacement around blade mid-chord in time is adopted.
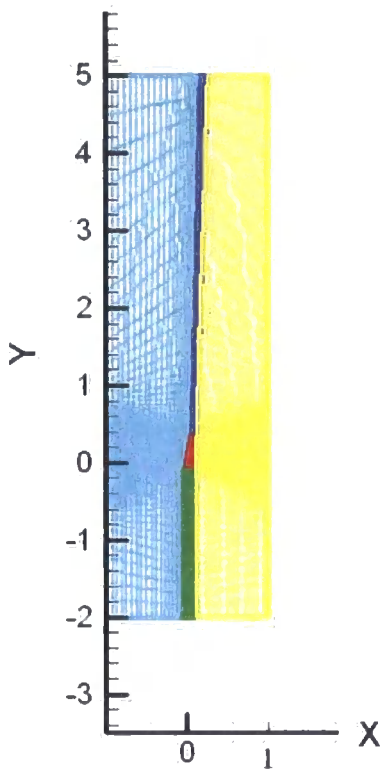
46

Figure 5.7 One Blade 2D Simulation

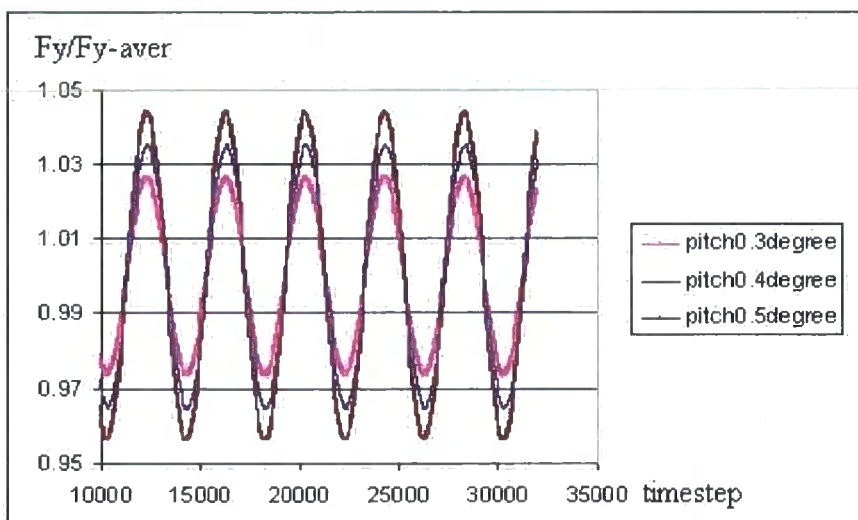Figure 5.8 shows the non-dimensional blade force variation under given different pitch angle.

Figure 5.8 Non-Dimensional Force Comparisons with Different Pitch Angle

Table 5.2 shows the non-dimensional force variation percentage with different pitch angle.

Table 5.2 Non-dimensional Force Comparisons with Different Pitch Angles

Pitching angle	FY_{min}/FY_{av}	FY_{max}/FY_{av}	Variation percentage
0.3degree	0.974	1.026	5.30%
0.4degree	0.965	1.035	7.06%
0.5degree	0.956	1.044	8.81%

From the value of Table 5.2, it can be seen that the force variation percentage is proportional to the pitching angle which means this relationship is liner. Therefore, in order to minimize the force variation caused by the blade-tower interaction, the correct pitching angle can be obtained by interpolation or extrapolation method in terms of different variation percentage.

In a given condition, the force variation caused by the blade-tower interaction is expressed by the Figure 5.9.
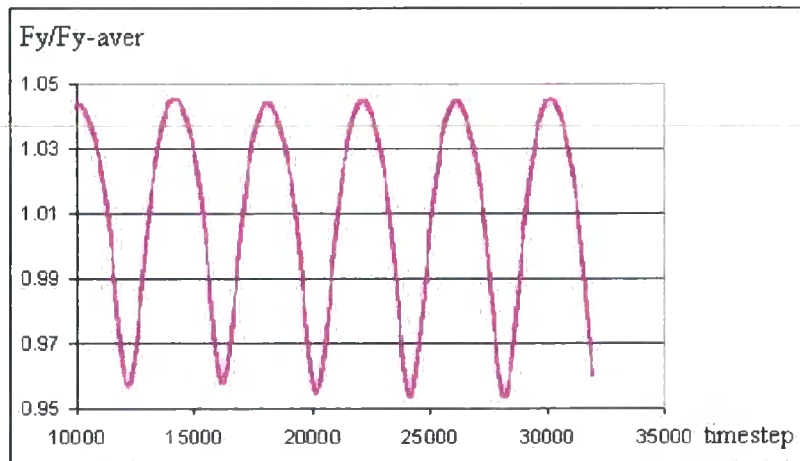

Figure 5.9 Non-Dimensional Force Variation in Tangential Direction Caused by Blade-Tower Interaction

Figure 5.9 show the non-dimensional minimum force in tangential direction is 0.953; the non-dimensional maximum force in tangential direction is 1.047, the force variation percentage is 9.34%. In order to minimize this variation, linear

extrapolation method is adopted to get the suitable pitch angle based on the database shown in Table 5.2. The calculated pitching angle is 0.53° to generate the same force variation percentage (9.34%) but out of phase which is shown in Figure 5.10. If pitch angle is larger than 0.53°, the force variation generated by pitching blade will be larger than which shown in Figure 5.9 and the force variation can not be minimized.
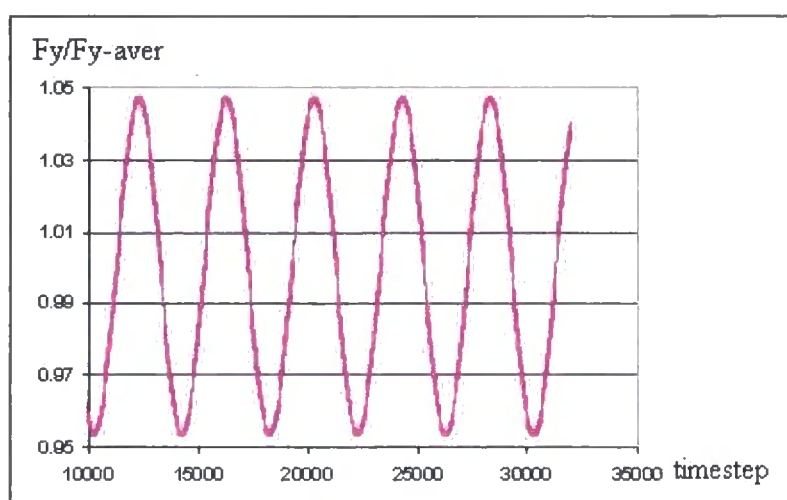

Figure 5.10 Blade Force Variation Caused by Pitching Blade 0.53°

In order to cancel the force variation caused by the blade-tower interaction (as shown in Figure 5.9) by that caused by the blade pitching (Figure 5.10), the correct phase angle has to be chosen to make the two curves just in the opposite phase, which means the start point to pitch the blade has to be chosen also. In this case, the two curves' time step difference measured from Figure 5.9 and Figure 5.10 is 70 when they are just in the opposite phase. The time step for one revolution is 4000, therefore, the difference phase angle is 360x70/4000=6.3°. Through running the MB3D code, it is calculated that the time to pass the whole domain is 0.1337 sec, thus it can be deduced that the pitching start time is 0.1337x6.3/360=0.00234 sec, which is almost the same moment when the blade just passing the tower. Now, the pitching blade can be added onto the blade-tower computational domain and the pitching effect on the blade force will be analysed while the rotating blade is periodically pitched. Figure 5.11 and Table 5.3 showed the non-dimensional force variations.
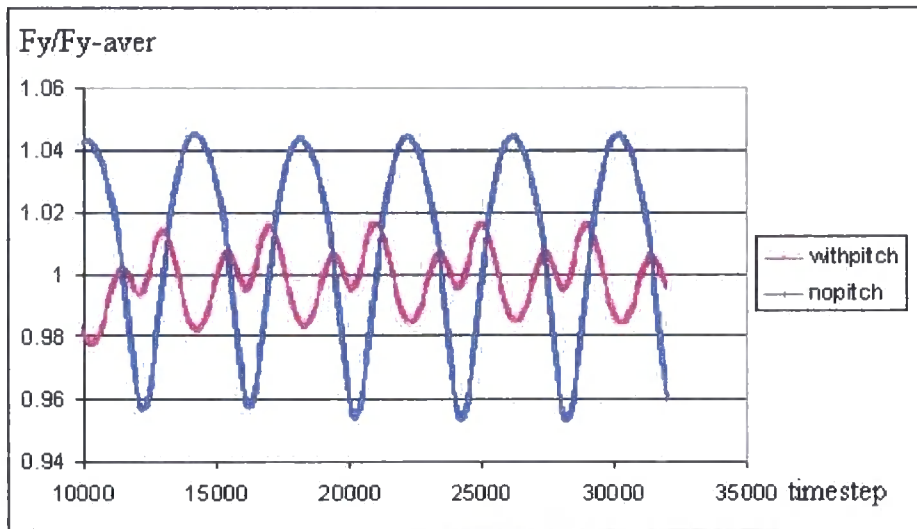
Figure 5.11 Non-Dimensional Tangential Force Comparisons With and Without Pitching Blade

Table 5.3 Non-dimensional Tangential Force Comparisons

Non-dimensional Force	$FY_{min}/$ FY_{av}	$FY_{max}/$ FY_{av}	Variation percentage
Without blade pitching	0.953	1.047	9.34%
With blade pitching	0.983	1.017	3.31%

Figure 5.11 and Table 5.3 showed, after the adaptive pitching is added, the blade force variation in the tangential direction is reduced by (9.34-3.31)/9.34=65%. It can not be totally cancelled, since the force variation caused by the blade-interaction is not of a pure sinusoidal form, while the force variation caused by pitching the blade is almost of a pure sinusoidal form, therefore, just part of the variation can be cancelled due to the different displacement form. However, it can be seen that just a little pitching can reduce most of the unsteady force from the blade-tower interaction.

Based on the analysis above, the blade force variation caused by the blade-tower interaction can be well simulated by the MB3D code. And the pitch active

control effect on the blade-tower interaction is commendably simulated as well. Till now, this analysis is based on one blade assumption. In reality, most wind-turbines have three rotor blades. In the following section, the three blades situation is simulated by MB3D code.

5.3 Three Blades Adaptive Pitching for Active Control

In order to study on the pitching blade effect, three blades with one tower were simulated in a 2D situation. Figure 5.12 and Figure 5.13 show the computational domain.

In this simulation, 20 blocks were used in the computation domain. The wind speed is assumed to be 15m/s, the diameter of the tower is 1m, the blade (mid-chord) and tower (leading edge) distance is 1.3m, and the tangential speed of the blade is defined to be 1.75m/s to make the flow incidence angle close to zero. When the blades are rotating, the forces on all the three blades are changing due to the blade-tower interaction. But the unsteady flow pattern is the same for all three blades, with a constant phase difference. The middle one blade is chosen to be as the reference to study the blade force variation. For one revolution, the time step is 4000. In order to minimize the force variation caused by the blade-tower interaction, the force curve caused by the interaction has to be analyzed first; then the correct pitching regulation is chosen to match it.
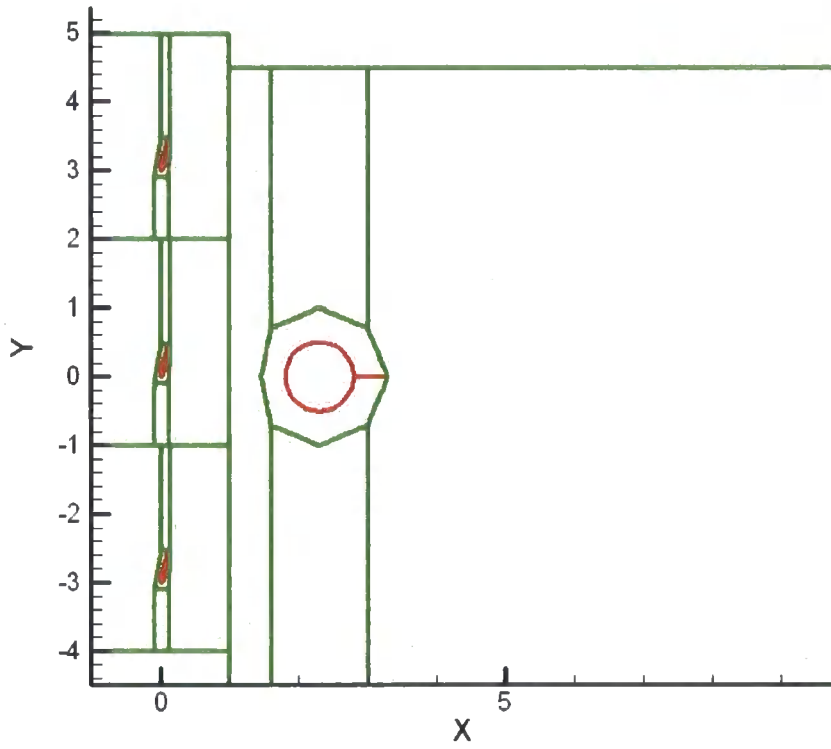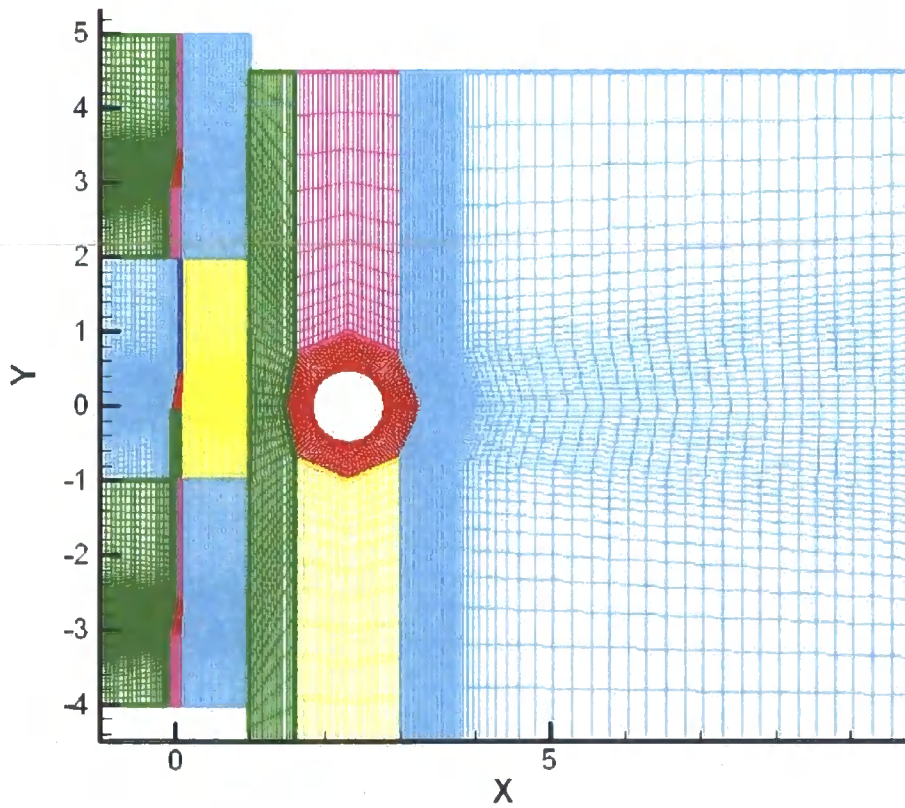
Figure 5.12 Three Blades and Tower in 2D Situation

Figure 5.13 Three Blades and Tower 2D Mesh

(1) Axial Force

Figure 5.14 shows the force (axial direction) variation in five revolutions. The top curve shows clearly how the blade force varies with different blade tower relative position. As the blade approaches the tower, the force on the aerofoil falls until the blade is just in front of the tower; as the blade then proceeds to pass the tower, the generated force on the aerofoil rises and then returns to the normal condition.

In order to minimize this interaction, the blade can be designed to start to pitch at a circumferential point when the blade is just about to pass the tower and stop pitching at a point when the blade has past the tower. This force curve in the axial direction caused by just pitching the blade is also shown in Figure 5.14.
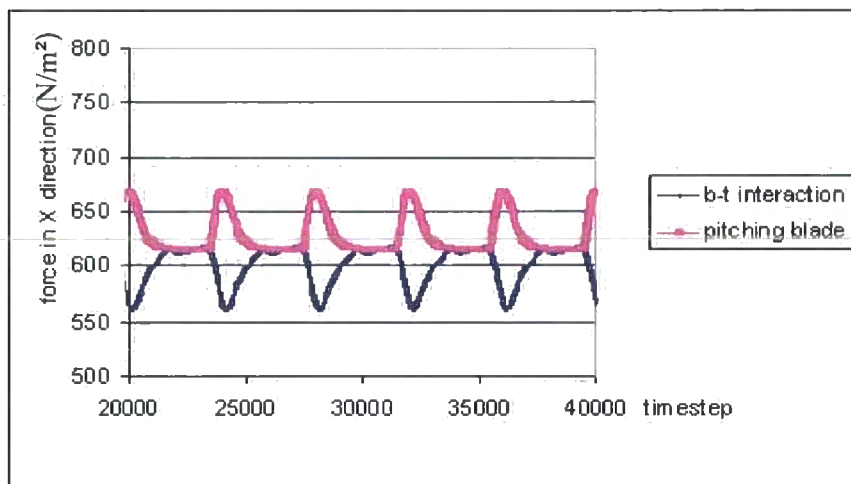

Figure 5.14 Axial Blade Force Comparisons

According to the analysis of the force variation (by blade-tower interaction) curve in Figure 5.14, it can be measured that the force starts to variation based on sinusoidal form from the 3000 time step till 4700 time step in each revolution, which means, the blade can be set to start pitching when the blade-tower angle is

(4000-3000)x360/4000=90° as the blade approaches the tower, and stop pitching when the blade is past the tower with a blade-tower angle (4700-4000)x360/4000=63°, and thus the correct phase opposite curve is obtained. Based on the numerical test and interpolation or extrapolation methods which are described in section 5.2, 0.4°pitch angle is chosen to match the force variation curve amplitude. Under this condition, the force variation on the pitching blade is simulated and shown in Figure 5.14 as the bottom curve. Based on the two curves shown in Figure 5.14, the pitching blade is added to the blade-tower computational domain and new blade force variation is calculated. Figure 5.15, Figure 5.16 and Table 5.4 showed the pitching effect on the force variation.
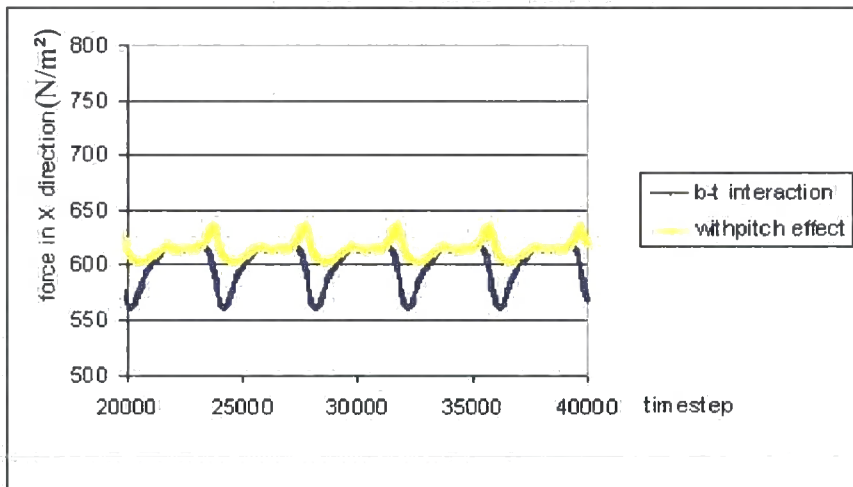

Figure 5.15 Axial Force Comparisons With and Without Pitching Blade

Figure 5.16 Non-Dimensional Axial Force Comparisons With and Without
Pitching Blade

Table 5.4 Non-dimensional Axial Force Comparisons

Non-dimensional Force	$FX_{min}/$ FX_{av}	$FX_{max}/$ FX_{av}	Variation percentage
Without blade pitching	0.951	1.049	9.75%
With blade pitching	0.973	1.027	5.37%

Figure 5.15, 5.16 and Table 5.4 show that the axial force variation was reduced from 9.75% to 5.37%, which means it is reduced by 5.37/9.75=55.07% through using the adaptive pitching blade. This is useful for reducing the bending moment variation, significant to the wind-turbine structure integrity.

(2) Tangential Force

In the same situation, the force in the Y-direction is analyzed. Figure 5.17 shows the tangential force variation. When the blades pass the tower, the force in Y-direction has the same regulation as it is in X-direction. The tangential force variation not only increases the power output fluctuation, but also reduces the average power output.

55

Also, under the same pitching regulation (the blade starts pitching when the blade-tower angle is 90° before it pass the tower, and stops pitching when the blade past the tower with blade-tower angle 63°, and the blade is pitched based on the sinusoidal form with 0.4° pitch angle) The pitching effect is shown in Figure 5.18, 5.19 and Table 5.5 as follows.
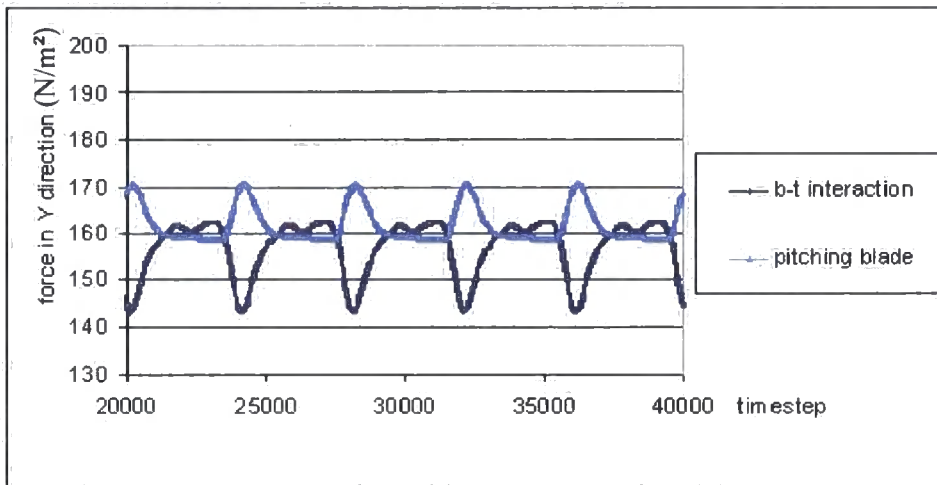
Figure 5.17 Tangential Blade Force Comparisons
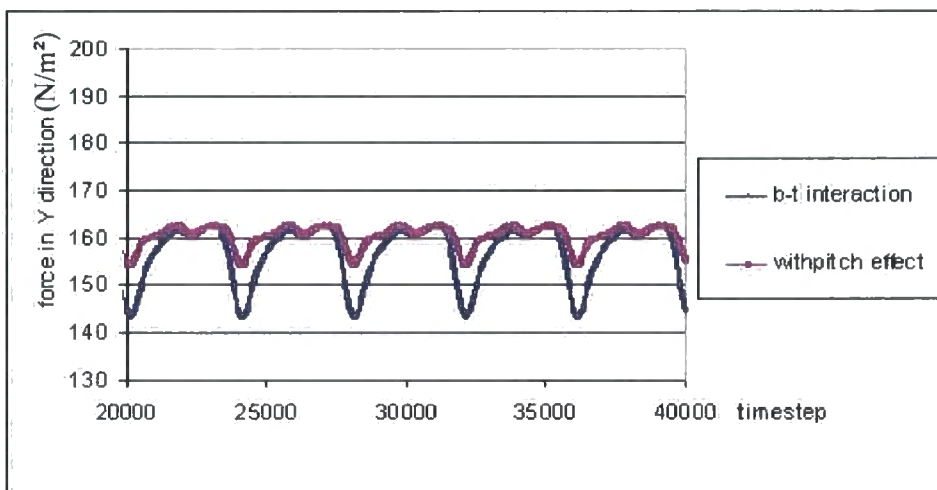
Figure 5.18 Tangential Force Comparisons With and Without Pitching Blade
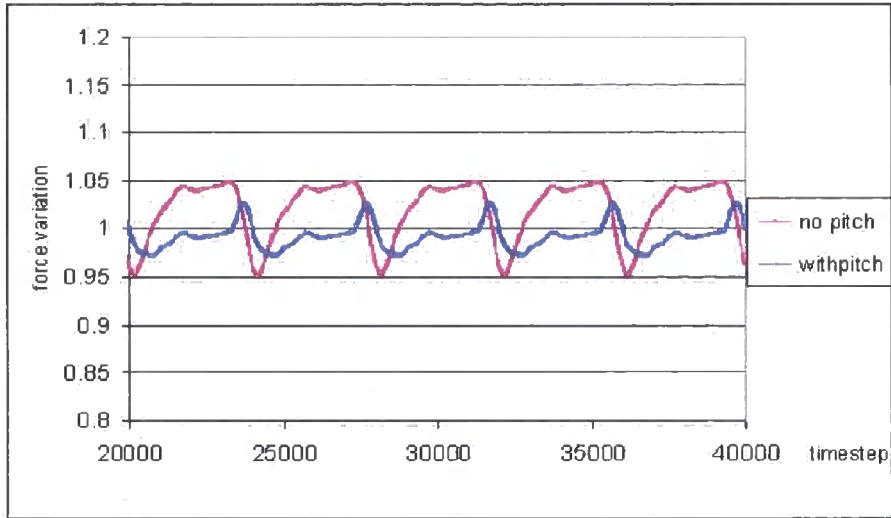
56
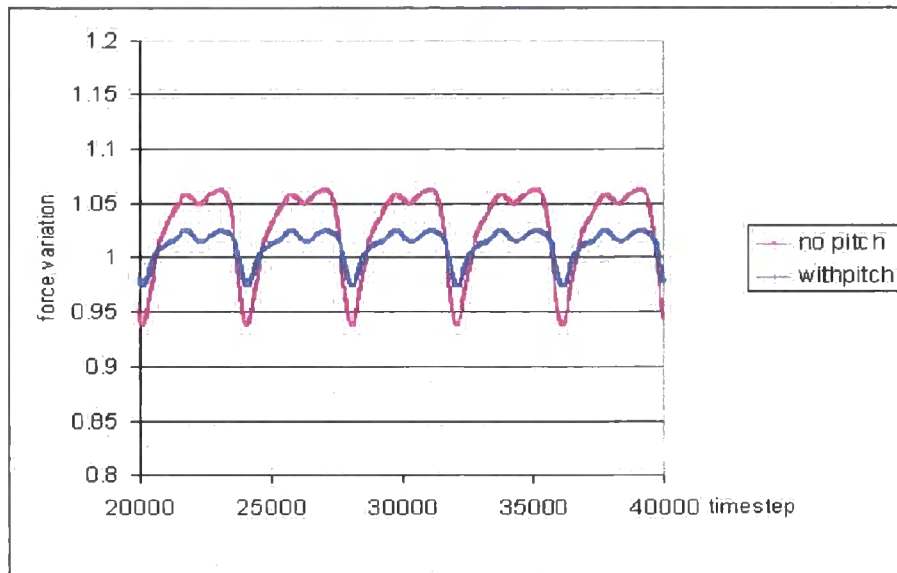
Figure 5.19 Non-Dimensional Tangential Force Comparisons With and Without
Pitching Blade

Table 5.5 Non-dimensional Tangential Force Comparisons

Non-dimensional Force	$FY_{min}/$ FY_{av}	$FY_{max}/$ FY_{av}	Variation percentage
Without blade pitching	0.93702	1.06298	12.60%
With blade pitching	0.97386	1.02614	5.23%

In this situation, from Figure 5.19 and Table 5.5, it can be seen that after adding
the blade pitching, the tangential force variation is decreased from 12.6% to
5.23% which means it is decreased by 5.23/12.6=58.49%. From Figure 5.18, it
can be seen that the average tangential force is increased from 154 to 160 which
means it is increased by (160-154)/160=3.75%. Therefore the average power
output for this blade section should be increased by 3.75%.

5.4 Summary

In this chapter, the wind turbine blade tower interaction and adaptive blade pitching control are studied. The blade force variations caused by the blade-tower interaction are simulated under different blade-tower gap distances using CFD simulation method. A remarkable decrease on blade force variation is achieved by the application of sinusoidal regulation applied to the blade adaptive pitching control, for given relative angles between the blade and tower. In the simulation cases, when pitching the blade just $0.5°$ under the sinusoidal pitching displacement in time, the force variation is reduced by 50%. This result displays the noticeably pitching effects of the adaptive control on the blade-tower interaction. Therefore, a good resolution is provided to minimize the blade force variations caused by the blade-tower interaction.

The simulation results demonstrate the effectiveness of the MB3D code to simulate 2D situation, therefore, this code can be developed and applied to simulate the 3D situation, which will provide guidance to engineers to minimize the blade bending momentum and improve the wind turbine structure stability for a range of power generation. The increased capital and exploitation costs due to the introduction of periodically blades pitching mechanism into the wind turbine design should be considered also.

CHAPTER 6 CONCLUSIONS AND RECOMMENDATIONS

· In this thesis, CFD MB3D code was introduced to simulate the fan tone noise wave transmission along the duct upstream and the pitching blade application in wind turbine to minimize the blade-tower interaction.

6.1 Conclusions on the Fan Tone Noise Analysis

In Chapter 4, the CFD MB3D code has been used to simulate the different pressure wave transmissions for the different applied driving frequencies. The simulation result shows, when the applied driving frequency is above the cut-off frequency, the pressure wave will propagate along the duct axial direction upstream. When the applied driving frequency is blow the cut-off frequency, the pressure wave will decay along the duct. The rate of the decay will increase as the cut-off ratio is decreased. In this paper, the different cut-off ratio 60.60% & 30.3% are simulated, the results display that the pressure wave decayed faster under 30.3% cut-off ratio condition.

Based on the simulation results, it can be seen that the acoustic waves can be simulated by the CFD MB3D code with low numerical dispersion and dissipation in 2D situation. There is no experimental result available so far, but this simulation gives an advantage for the future to do comparison with experimental/theoretical results. Also, this CFD simulation method provides an advantage for simulating pressure wave transmissions on a concentric cylindrical

duct in 3D situation. A phenomenon of 3D simulation of a concentric cylindrical duct is the part span cut-on and part span cut-off situations. These situations are the results of the cut-on case at a given radius occurring simultaneously with the cut-off case at a different radius. A further advantage of the CFD MB3D code simulation allows us to develop empirical models to analyse pressure wave transmissions under a non-axisymmetric flow.

The results of the simulation can be used in the selection of the following:

- Number of rotor blades
- Rotor and stator combination
- Tip-hub ratio
- Rotor tip Mach number

All of the above factors can be used, at the design stage, to determine cut-off situation avoiding cut-on situation and hence minimize the fan tone noise propagation.

6.2 Conclusions on the Analysis of Wind Turbine Blade-Tower Interaction

In chapter 5, the wind turbine blade-tower interaction and blade adaptive pitching control are simulated using CFD MB3D code. The calculation results showed that the blade force variation caused by the blade-tower interaction can be minimized through introducing adaptive pitching control on the blade.

In the 2D simulation cases, when pitching the blade just 0.5° by applying the sinusoidal regulation on the adaptive control under given blade pitching start/stop circumferential points in the revolutions, the force variation is reduced by 50%. This result displays the noticeably pitching effects of the adaptive control on the blade-tower interaction. A 50% decrease on blade force variation

60

can be achieved based on the simulation results. Thus, it provides a good resolution to minimize the blade-tower interaction.

The results demonstrate the CFD MB3D code can be applied to simulate the wind turbine blade-tower interaction in 2D situation. Therefore, this method provides an advantage for doing the 3D calculations.

The simulation results can be used to provide guidance to engineers on how to minimize the blade-tower interaction. Consequently, it will contribute to the following:

- Minimize the blade bending momentum.
- Increase the blade fatigue life span.
- Improve the wind turbine structure stability.
- Reduce the aerodynamic noise caused by the blade-tower interaction.

6.3 Recommendations

Based on the analysis above, some recommendations are provided below:

- For the fan noise transmission problem, it is recommended to simulate the resonance situation.
- More research should be carried out in 3D simulations, and to predict the noise level for realistic fan configurations.
- In wind turbine pitching blade, the 3D situation is recommended to be studied and the pitching regulation should be improved in order to minimize the blade-tower interaction.
- The aeroelastic behaviour of the blade will cause the change of attack angle by blade deflection. Further simulation should be studied on this change and the effect on the blade-tower interaction.

61

BIBLIOGRAPHY

Anderson J. D., Jr., "*Computational Fluid Dynamics: The Basics with Applications*", McGraw-Hill, Inc. 1995.

Ansley W. M., "*Unsteady Loading on Wind Turbines due to Blade-Tower Interaction*", University of Durham, 2002.

Baldwin B.S., and Barth T. J., "*A One-Equation Turbulence Transport Model for High Reynolds Number Wall Bound Flows*", NASA Technical Memorandum 102847, 1991.

Baldwin B.S., and Lomax H., "*Thin Layer Approximation and Algebraic Model for Separated Turbulent Flows*", AIAA Paper 78-257, 1978.

Denton J.D., "*The Calculation of Three-Dimensional Viscous Flow Through Multistage Turbomachines*", Transactions of the ASME, Journal of Turbomachinery, Vol.114, P.18-26, 1992.

Dixon S. L., "*Fluid Mechanics, Thermodynamics of Turbomachinery*", Third Edition, Pergamon Press Ltd, 1978.

Duque E. P. N. and Dame C. P. V., et al., "*Navier-Stokes simulations of the NREL combined experimental Phase II Rotor*", European Wind Energy Conference, Nice, France, 1999.

Duque E. P. N. and Johnson W., et al., "*Numerical Predictions of Wind Turbine Power and Aerodynamic Loads for NREL Phase II Combined Experiment Rotor*", AIAA paper 2000-0038, 2000.

Envia E., Wilson A. G. and Huff D. L., "*Fan Noise: A Challenge to CAA*", International Journal of Computational Fluid Dynamics, Vol.18, No.6, P.471-480, 2004.

Farret F. A., Pfischer L. L., Bernardor D. P., "*Active Yaw Control with Sensorless Wind Speed & Direction Measurements for Horizontal Axis Wind Turbines* ", Third IEEE International Caracas Conference, pp. I25/1-I25/6, 2000.

Freund J. B., Lele S. K., and Moin P., "*Direct Simulation of a Mach 1.92 Jet and Its Sound Field*", AIAA Paper 98-2291, 4th AIAA/CEAS Aeroacoustics Conference, Toulouse, France, 1998.

Giles M. B., "*Nonreflecting Boundary Conditions for Euler Equation Calculations*", AIAA Journal, Vol.28, No.12, P.2050-2058, 1990.

Giles M. B., "*Calculation of Unsteady Wake Rotor Interaction*", AIAA Journal of Propulsion and Power, Vol.4, No.4, 1988.

Gipe P., "*Wind Power: Renewable Energy for Home, Farm, and Business*", Chelsea Green Publishing Company, 2004.

Goldstein M. E., "*Aeroacoustics*", McGraw-Hill, Inc. 1976.

Hall K. C. and Lorence C. B., "*Calculation of Three-Dimensional Unsteady Flows in Turbomachinery Using the Linearized Harmonic Euler Equations*", ASME, Paper 92-GT-136, 1992.

Hansen M. O. L., *"Aerodynamics of Wind Turbines"*, James & James (Science Publishers) Ltd., 2000.

Hanson D. B., *"Coupled Two-Dimensional Cascade Theory for Noise and Unsteady Aerodynamics of Blade Row Interactions in Turbofans"*, NASA CR-4506, 1994.

He L., *"A New Two-Grid Acceleration Method for Unsteady Navier-Stokes Calculations"*, AIAA Journal, Vol.30, No.12, 1993.

He L., *"Fourier Modelling of Steady and Unsteady Nonaxisymmetrical Flows"*, AIAA, Journal of Propulsion and Power, Vol.22, No.1, P.197-201, 2006.

He L., *"Computational Fluid Dynamics"*, lecture notes, University of Durham, 2006.

Heller H. H., *"DLR's Involvement in European Aviation Noise Research on Fixed and Rotary Wing Aircraft"*, Fifth AIAA/CEAS Aeroacoustics Conference Keynote Lecture, 1999.

Holmes D. G. and Lorence C. B., *"Three Dimensional Linearized Navier-Stokes Calculations for Flutter and Forced Response"*, Proceeding of the 8th International Symposium on Unsteady Aerodynamics and Aeroelasticity of Turbomachines, Stockholm, Sweden, 1997.

Huang X. Q., *"Three-Dimensional Unsteady Flow in Oscillating Turbine Blade Row"*, University of Durham, PhD Thesis, Chapter 2 and Chapter 4, 2006.

Jeon W., *"A Numerical Study on the Effects of Design Parameters on the Performance and Noise of a Centrifugal Fan"*, Journal of Sound and Vibration, Vol.265, No.1, P.221-230, 2003.

Kang S. and Hirsch C., "*Numerical Investigation of the 3D Flow Around NREL Untwisted Wind Turbine Blades*", Turbomachinery Fluid Dynamics and Thermodynamics, Firenze Italy, 2001

Larsson J., "*Computational Aero Acoustics for Vehicle Applications*", Chalmers University of Technology, Sweden, PhD Thesis, 2002.

Maaloum A., Kouidri S., Bakir F., Rey R., "*Effect of Inlet Duct Contour and Lack Thereof on the Noise Generated of an Axial Flow Fan*", Applied Acoustics, Vol.64, No.10, P.999-1010, 2003.

Morreti G., Abbett M., "*A Time-Dependent Computational Method for Blunt Body Flows*", AIAA Journal, Vol. 4, No 12, pp.2136-2141, 1966.

Muljadi E.; Butterfield C. P., "*Effect of Turbulence on Power Generation for Variable Speed Wind Turbines*", ASME Wind Energy Symposium, Houston, TX, Jan. 6-9, 1997.

Muljadi E., Pierce K., Migliore P., "*Control Strategy for Variable-Speed, Stall-Regulated Wind Turbines*", American Controls Conference, Philadelphia, PA, 1998.

Ning W., "*Computational of Unsteady Flow in Turbomachinery*", University of Durham, PhD Thesis, Chapter 2, 1998.

Pedersen E., Halmstad H., "*Noise Annoyance from Wind Turbines-a Review*", Swedish Environmental Protection Agency Report 5308, 2003.

Polacsek C., Desbois-Lavergne F., "*Fan Interaction Noise Reduction Using a Wake Generator: Experiments and Computational Aeroacoustics*", Journal of Sound and Vibration, Vol.265, No.4, P.725-743, 2003.

Rumsey C. L., Biedron R. T., Farassat F. and Spence P. L., "*Ducted-Fan Engine Acoustic Predictions Using a Navier-Stokes Code*", Journal of Sound and Vibration, Vol.213, No.4, P.643-664, 1998.

Sato K., "*Blade Row Interaction in Radial Turbomachines*", University of Durham, PhD Thesis, Chapter 3, 1999.

Schepers J.G., Brend A. J., "*Final report of IEA Annex XIV: Field rotor aeronautics*", ECN-C-97-027, 1997.

Shieh C. M., and Morris P. J., "*Parallel Numerical Simulation of Subsonic Cavity Noise*", AIAA Paper 99-1981, 5th AIAA/CEAS Aeroacoustics Conference, Bellevue, Washington.

Smith S. N., "*Discrete Frequency Sound Generation in Axial Flow Turbomachines*", British Ministry of Defence Report R&M No.3709, 1973.

Spalart P. R., Allmaras S. R., "*A one-equation turbulence model for aerodynamic flows*", AIAA paper 92-0439, 1992.

TAM C.K.W., "*Computational Aeroacoustics: An Overview of Computational Challenges and Applications*", International Journal of Computational Fluid Dynamics, Vol.18, No.6, P.547-567, 2004.

Tyler J. M. and Sofrin T. G., "*Axial Flow Compressor Noise studies*", SAE Transactions Vol.70, P. 309-332, 1962.

Van der Hooft E. L. and van Engelen T. G., "*Estimated Wind Speed Feed Forward Control for Wind Turbine Operation Optimisation*", European Wind Energy Conference, London, 2004.

Van den Berg G. P., *"Do Wind Turbines Produce Significant Low Frequency Sound Levels?"*, 11th International Meeting on Low Frequency Noise and Vibration and its Control, Maastricht The Netherlands, 2004.

Ventres C. S., Theobald M. A. and Mark W. D., *"Turbofan Noise Generation: Volume 1: Analysis"*, NASA CR-167952, 1982.

Weidemann J., *"Analysis of the Relation Between Acoustic and Aerodynamics Parameters for a Series of Dimensionally Similar Centrifugal Fan Rotors"*, NASA TT F-13, P.798, 1971.

Wong Y. J., Paurobally R., Pan J., *"Hybrid Active and Passive Control of Fan Noise"*, Applied Acoustics, Vol.64, No.9, P.885-901, 2003.

Zheng Y., *"Computational Aerodynamics on Unstructured Meshes"*, PhD Thesis, University of Durham, 2004.